

# Constraints on CP-violating gauge-Higgs operators

Siddharth Dwivedi<sup>1\*</sup>, Dilip Kumar Ghosh<sup>2†</sup>, Biswarup Mukhopadhyaya<sup>1‡</sup> and Ambresh Shrivastava<sup>1§</sup>

<sup>1</sup>*Regional Centre for Accelerator-based Particle Physics, Harish-Chandra Research Institute, Chhatnag Road, Jhansi, Allahabad - 211019, India*

<sup>2</sup>*Department of Theoretical Physics, Indian Association for the Cultivation of Science, 2A & 2B Raja S.C. Mullick Road, Kolkata - 700032, India*

October 8, 2018

## Abstract

We consider the most general set of  $SU(2) \times U(1)$  invariant CP-violating operators of dimension six, which contribute to  $VVh$  interactions ( $V = W, Z, \gamma$ ). Our aim is to constrain any CP-violating new physics above the electroweak scale via the effective couplings that arise when such physics is integrated out. For this purpose, we use, in turn, electroweak precision data, global fits of Higgs data at the Large Hadron Collider and the electric dipole moments of the neutron and the electron. We thus impose constraints mainly on two-parameter and three-parameter spaces. We find that the constraints from the electroweak precision data are the weakest. Among the existing Higgs search channels, considerable constraints come from the diphoton signal strength. We note that potential contribution to  $h \rightarrow \gamma Z$  may in principle be a useful constraining factor, but it can be utilized only in the high energy run. The contributions to electric dipole moments mostly lead to the strongest constraints, though somewhat fine-tuned combinations of more than one parameter with large magnitudes are allowed. We also discuss constraints on gauge boson trilinear couplings which depend on the parameters of the CP-violating operators.

HRI-RECAPP-2015-009

---

\*E-mail: siddharthdwivedi@hri.res.in

†E-mail: tpdkg@iacs.res.in

‡E-mail: biswarup@hri.res.in

§E-mail: ambreshkshrivastava@hri.res.in

# 1 Introduction

Although the discovery of “a Higgs-like boson” at the Large Hadron Collider (LHC) has been a refreshing development [1, 2], there is no clear signal yet for physics beyond the standard model (SM). It is therefore natural that physicists are trying to wring the last drop out of the Higgs sector itself, in attempts to read fingerprints of new physics.

One approach is to examine all available data in terms of specific new models, such as supersymmetry or just additional Higgs doublets. In the other approach, one can take a model-independent stance, parametrize possible modifications of the interaction terms of the Higgs with pairs of SM particles, and examine them in the light of the available data. Such modifications can again be of two types. In the first category, they are just multiplicative modifications of the coupling strengths, the Lorentz structures remaining the same as in the SM. Constraints on such modifications have already been derived from the available Higgs data [3–7]. In the second class, one considers additional operators with new Lorentz structures satisfying all symmetries of the SM [8–15]. Gauge invariance of such operators in their original forms may be expected, since they are obtained by integrating out new physics that is just above the reach of the present round of experiments. Sets of such higher-dimensional operators contributing to the effective coupling of the Higgs to, say a pair of electroweak vector bosons have been studied extensively. Here it makes sense to include only  $SU(2) \times U(1)$  invariant operators in one’s list to start with, because the yet unknown new physics lies at least a little above the electroweak symmetry breaking scale. A host of such gauge invariant higher-dimensional operators have been, and are being, analyzed with considerable rigor, and now there exist limits on them, using data ranging from electroweak precision measurements to global fits of LHC results [16–49].

Most of such analyses include higher-dimensional operators that conserve charge conjugation (C), parity (P) and time-reversal (T). However, there is evidence of C, P and CP-violation in weak interactions [50], and there are speculations about other sources of CP-violation as well, especially with a view to explaining the baryon asymmetry in our universe [51, 52]. The possibility of CP-nonconservation cannot therefore be ruled out in the new physics currently sought after. Thus one may in principle also obtain higher-dimensional interaction terms involving the Higgs and a pair of gauge bosons. The constraints on such terms, and identification of regions in the parameter space where they can be phenomenologically significant, form the subject-matter of the present paper.

The CP-violating effective couplings, interestingly, are not constrained by the oblique electroweak parameters at one-loop level up to  $\mathcal{O}(\frac{1}{\Lambda^2})$ , where  $\Lambda$  is the cutoff scale of the effective theory. The leading contributions to self-energy corrections to electroweak gauge bosons at one-loop level occur at  $\mathcal{O}(\frac{1}{\Lambda^4})$ . Therefore, electroweak precision (EWP) data are not expected to provide severe constraints on CP-odd parameters. In addition to this, Higgs-mediated event rates in various channels receive contributions from these couplings at  $\mathcal{O}(\frac{1}{\Lambda^4})$ . Thus they can also be constrained from global fits of the LHC data. The strongest limits on them, however, arise from the contributions to the electric dipole moments (EDMs) of the neutron and the electron, both of which are severely restricted from experiments. As we shall see in the following sections, a single CP-violating operator taken at a time may in certain cases be limited to a very small strength from the above constraints, while two or three such operators considered together can have relatively larger, but highly correlated coefficients. Some of these operators can have interesting phenomenological implications, especially in the context of the LHC.

A study in similar lines can be found in Refs. [42, 45–47, 49]. However, we have performed the most comprehensive analysis, taking all the five possible dimension-6 CP-violating  $VVh$  operators ( $V = W, Z, \gamma$ ), which are not yet discussed thoroughly in the literature. We provide the constraints obtained from the oblique electroweak parameters. The constraints coming from global fits of LHC

data and electric dipole moments, for two and three operators taken at a time, have been compared. In addition to these we also provide the constraints on trilinear gauge boson couplings coming from LEP data on gauge boson pair production.

Our paper is organized as follows. In section 2, we provide details on the CP-violating gauge Higgs operators and derive Feynman rules for three point vertices of our interest. In section 3 we present the constraints on CP-violating parameters coming from the precision electroweak measurements. Following this, we perform a global analysis of these parameters using LHC data on Higgs in section 4 and we discuss EDM constraints on CP-violating parameters in section 5. Section 6 is devoted to discussion of results. Finally we summarize and conclude in section 7.

## 2 Morphology of CP-violating Gauge-Higgs Operators

In the effective Lagrangian approach that has been followed here, one can write a Lagrangian ( $\mathcal{L}_{\text{eff}}$ ) comprising only of the SM fields, where the effects of the new physics that appear above the cutoff scale  $\Lambda$  are encapsulated in higher dimensional gauge invariant operators. In general,

$$\mathcal{L}_{\text{eff}} = \sum_i \frac{f_i}{\Lambda^{d_i-4}} O^i, \quad (1)$$

where  $d_i > 4$  is the mass dimension of the operator  $O^i$  and the dimensionless free parameter  $f_i$  fixes the strength of the corresponding operator. The operators constructed out of the Higgs doublet and the  $SU(2) \times U(1)$  gauge fields are of even dimensions, and at the leading order they have mass dimension  $d_i = 6$ . The dimension six CP-even gauge invariant operators constructed out of the Higgs doublet ( $\Phi$ ) and the electroweak gauge fields ( $B_\mu, W_\mu^a$ ), that modify the gauge-Higgs couplings are given as follows:

$$\begin{aligned} O_W &= \frac{f_W}{\Lambda^2} (D_\mu \Phi)^\dagger \hat{W}^{\mu\nu} (D_\nu \Phi); \quad O_B = \frac{f_B}{\Lambda^2} (D_\mu \Phi)^\dagger \hat{B}^{\mu\nu} (D_\nu \Phi); \\ O_{BB} &= \frac{f_{BB}}{\Lambda^2} \Phi^\dagger \hat{B}^{\mu\nu} \hat{B}_{\mu\nu} \Phi; \quad O_{WW} = \frac{f_{WW}}{\Lambda^2} \Phi^\dagger \hat{W}^{\mu\nu} \hat{W}_{\mu\nu} \Phi; \\ O_{BW} &= \frac{f_{BW}}{\Lambda^2} \Phi^\dagger \hat{B}^{\mu\nu} \hat{W}_{\mu\nu} \Phi. \end{aligned} \quad (2)$$

In the above, we have defined  $\hat{B}_{\mu\nu} = i\frac{g'}{2} B_{\mu\nu}$  and  $\hat{W}_{\mu\nu} = i\frac{g}{2} \tau^a W_{\mu\nu}^a$ .  $g$  and  $g'$  are the electroweak coupling parameters corresponding to  $SU(2)$  and  $U(1)$  gauge groups respectively, and  $\tau^a$  ( $a = 1, 2, 3$ ) are the three Pauli matrices. We define the gauge covariant derivative as  $D_\mu \equiv \partial_\mu - i\frac{g}{2} \tau^a W_\mu^a - i\frac{g'}{2} Y B_\mu$ , where  $Y$  is the hypercharge quantum number. With this choice of the definition of gauge covariant derivative, field strength tensor  $W_{\mu\nu}^a$  is given by,  $W_{\mu\nu}^a = \partial_\mu W_\nu^a - \partial_\nu W_\mu^a + g\epsilon^{abc} W_\mu^b W_\nu^c$ . The constraints on CP-even parameters and their collider implications have been studied extensively in the literature [16, 21, 32, 36, 43, 44, 48]. In this work we are interested in corresponding CP-violating dimension six gauge-Higgs operators. These are,

$$\begin{aligned} \tilde{O}_W &= \frac{\tilde{f}_W}{\Lambda^2} (D_\mu \Phi)^\dagger \hat{\tilde{W}}^{\mu\nu} (D_\nu \Phi); \quad \tilde{O}_B = \frac{\tilde{f}_B}{\Lambda^2} (D_\mu \Phi)^\dagger \hat{\tilde{B}}^{\mu\nu} (D_\nu \Phi); \\ \tilde{O}_{BB} &= \frac{\tilde{f}_{BB}}{\Lambda^2} \Phi^\dagger \hat{\tilde{B}}^{\mu\nu} \hat{\tilde{B}}_{\mu\nu} \Phi; \quad \tilde{O}_{WW} = \frac{\tilde{f}_{WW}}{\Lambda^2} \Phi^\dagger \hat{\tilde{W}}^{\mu\nu} \hat{\tilde{W}}_{\mu\nu} \Phi; \\ \tilde{O}_{BW} &= \frac{\tilde{f}_{BW}}{\Lambda^2} \Phi^\dagger \hat{\tilde{B}}^{\mu\nu} \hat{\tilde{W}}_{\mu\nu} \Phi, \end{aligned} \quad (3)$$

Coupling	Effective coupling strength
$C_{WWh}$	$(-\tilde{f}_W - 2\tilde{f}_{WW})$
$C_{ZZh}$	$-1/c_W^2 \left[ c_W^2 \tilde{f}_W + s_W^2 \tilde{f}_B + 2(c_W^4 \tilde{f}_{WW} + s_W^4 \tilde{f}_{BB}) + 2s_W^2 c_W^2 \tilde{f}_{BW} \right]$
$C_{\gamma\gamma h}$	$-2s_W^2(\tilde{f}_{WW} + \tilde{f}_{BB} - \tilde{f}_{BW})$
$C_{\gamma Zh}$	$t_W/2 \left[ (-\tilde{f}_W + \tilde{f}_B) + 4(s_W^2 \tilde{f}_{BB} - c_W^2 \tilde{f}_{WW}) + 2c_{2W} \tilde{f}_{BW} \right]$
$C_{WW\gamma}$	$s_W/2(\tilde{f}_W + \tilde{f}_B + 2\tilde{f}_{BW})$
$C_{WWZ}$	$-s_W t_W/2(\tilde{f}_W + \tilde{f}_B + 2\tilde{f}_{BW})$

Table 1: CP-odd  $VVh$  and  $WWV$  coupling factors and their effective strengths.

where,  $\hat{W}^{\mu\nu} = \frac{1}{2}\epsilon^{\mu\nu\alpha\beta}\hat{W}_{\alpha\beta}$  and  $\hat{B}^{\mu\nu} = \frac{1}{2}\epsilon^{\mu\nu\alpha\beta}\hat{B}_{\alpha\beta}$ ,  $\epsilon^{\mu\nu\alpha\beta}$  being the four-dimensional fully antisymmetric tensor with  $\epsilon^{0123} = 1$ .

In principle, the CP-even operators [Eq.(2)] could have been assumed to exist simultaneously with the CP-odd ones considered here. However, such an approach generates far too large a set of free parameters, where the signature of the CP-violating effective couplings would be drowned. Moreover, the CP-even operators are independent of the CP-odd ones (and vice versa); therefore, setting them to zero is a viable phenomenological approach. We therefore postulate that the new physics above scale  $\Lambda$  is such that *only CP-violating dimension six effective operators are appreciable*, and the corresponding CP-conserving ones are much smaller. Such a “simplified approach,” we reiterate, is unavoidable for unveiling CP-violating high scale physics, as has been recognized in the literature [49, 53–55]. Studies focusing exclusively on the generation of CP-violating terms in specific new physics frameworks can also be found, an example being those in the context of extra space-time dimensions [56, 57].

Since we focus on the extension of the SM through the inclusion of the CP-odd operators only, the full BSM Lagrangian looks like,

$$\mathcal{L}_{\text{BSM}} = \mathcal{L}_{\text{SM}} + \tilde{O}_W + \tilde{O}_{WW} + \tilde{O}_B + \tilde{O}_{BB} + \tilde{O}_{BW}, \quad (4)$$

where  $\mathcal{L}_{\text{SM}}$  is the standard model Lagrangian. After the electroweak symmetry breaking, these

CP-odd operators contribute to following three-point vertices of our interest<sup>1</sup>,

$$\mathcal{L}_{WWh} = -\frac{gm_W}{\Lambda^2}(\tilde{f}_W + 2\tilde{f}_{WW})\epsilon^{\mu\nu\alpha\beta}k_{1\alpha}k_{2\beta}W_\mu^+(k_1)W_\nu^-(k_2)h(k), \quad (5)$$

$$\begin{aligned} \mathcal{L}_{ZZh} = & -\frac{gm_W}{\Lambda^2}\left[\frac{c_W^2\tilde{f}_W + s_W^2\tilde{f}_B}{c_W^2} + \frac{2(c_W^4\tilde{f}_{WW} + s_W^4\tilde{f}_{BB})}{c_W^2} + 2s_W^2\tilde{f}_{BW}\right] \\ & \epsilon^{\mu\nu\alpha\beta}k_{1\alpha}k_{2\beta}Z_\mu(k_1)Z_\nu(k_2)h(k), \end{aligned} \quad (6)$$

$$\begin{aligned} \mathcal{L}_{\gamma\gamma h} = & -2\left(\frac{gm_W}{\Lambda^2}\right)s_W^2(\tilde{f}_{WW} + \tilde{f}_{BB} - \tilde{f}_{BW}) \\ & \epsilon^{\mu\nu\alpha\beta}k_{1\alpha}k_{2\beta}A_\mu(k_1)A_\nu(k_2)h(k), \end{aligned} \quad (7)$$

$$\begin{aligned} \mathcal{L}_{\gamma Zh} = & \left(\frac{gm_W}{2\Lambda^2}\right)t_W\left[(-\tilde{f}_W + \tilde{f}_B) + 4(s_W^2\tilde{f}_{BB} - c_W^2\tilde{f}_{WW}) + 2c_W^2\tilde{f}_{BW}\right] \\ & \epsilon^{\mu\nu\alpha\beta}k_{1\alpha}k_{2\beta}A_\mu(k_1)Z_\nu(k_2)h(k), \end{aligned} \quad (8)$$

$$\begin{aligned} \mathcal{L}_{WW\gamma} = & \left(\frac{gm_W^2}{2\Lambda^2}\right)s_W(\tilde{f}_W + \tilde{f}_B + 2\tilde{f}_{BW}) \\ & \epsilon^{\mu\nu\alpha\beta}k_\beta W_\mu^+(k_1)W_\nu^-(k_2)A_\alpha(k), \end{aligned} \quad (9)$$

$$\begin{aligned} \mathcal{L}_{WWZ} = & -\left(\frac{gm_W^2}{2\Lambda^2}\right)(s_W t_W)(\tilde{f}_W + \tilde{f}_B + 2\tilde{f}_{BW}) \\ & \epsilon^{\mu\nu\alpha\beta}k_\beta W_\mu^+(k_1)W_\nu^-(k_2)Z_\alpha(k). \end{aligned} \quad (10)$$

In the above equations  $s_W = \sin\theta_W$ ,  $c_W = \cos\theta_W$ ,  $t_W = \tan\theta_W$ , and  $c_{2W} = \cos 2\theta_W$ , where  $\theta_W$  is the Weinberg angle. Here  $k$ s are the four-momenta of the fields that enter the vertex. We have taken all momenta to be inflowing toward the three-point vertex in establishing the Feynman rules. From the list of CP-odd interaction vertices shown above, one can observe a general tensor structure of the form  $\epsilon^{\mu\nu\alpha\beta}k_{1\alpha}k_{2\beta}$  in  $VVh$  vertices and a general tensor structure of the form  $\epsilon^{\mu\nu\alpha\beta}k_\beta$  in trilinear gauge boson couplings ( $WWV$ ). Because of this the CP-odd couplings are linear combinations of the parameters  $\tilde{f}_i$ . Note that we have not included the CP-odd operator involving gluon-Higgs coupling,

$$\tilde{O}_{GG} = \frac{\tilde{f}_{GG}}{\Lambda^2}\Phi^\dagger \hat{G}^{\mu\nu} \hat{G}_{\mu\nu} \Phi. \quad (11)$$

This operator introduces a  $\theta_{QCD}$  term [58, 59], and it is severely constrained by the experimental measurement of neutron EDM [50]. In Table 1, we list various couplings and their effective strengths ignoring the overall dimension full factor of  $\frac{gm_W}{\Lambda^2}$  in  $C_{VVh}$  and the dimensionless factor of  $\frac{gm_W^2}{\Lambda^2}$  in  $C_{WWV}$  couplings. Note that only  $ZZh$  and  $\gamma Zh$  couplings receive contribution from all five CP-odd operators. The operators which contribute to  $WW\gamma$  also contribute to  $WWZ$  and these couplings are related by,  $C_{WWZ} = -t_W C_{WW\gamma}$ .

### 3 Constraints from Electroweak Precision (EWP) Data

We note that unlike some of the CP-even (D=6) operators, the CP-odd operators do not contribute to the gauge boson propagator corrections at tree level, hence are not expected to receive severe

<sup>1</sup> The CP-odd operators considered here also contribute to four-point and five-point vertices like  $VVhh$ ,  $VVVh$  and  $VVVhh$ . However, as we will see in following sections, all the observables used in our analysis are sensitive to only three-point vertices at the leading order.

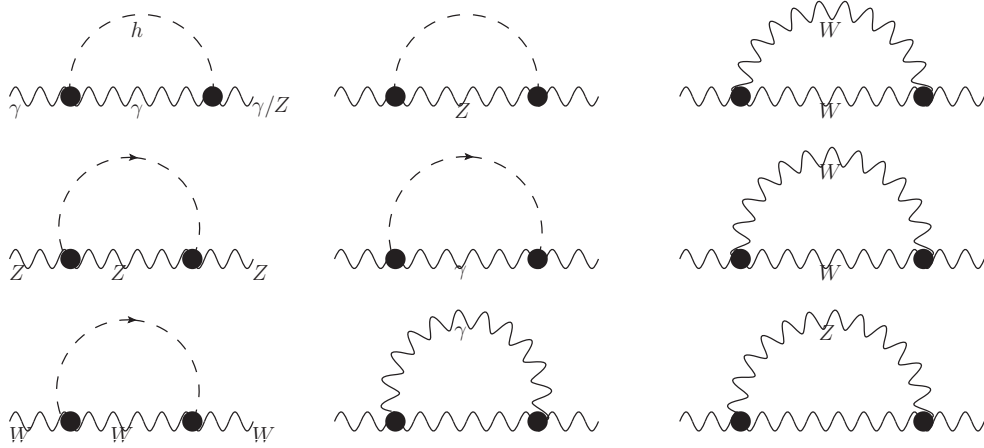


Figure 1: One-loop self energy corrections to electroweak vector bosons (oblique corrections) in presence of CP-odd operators. The blobs show the effective CP-odd vertices. These corrections are of  $\mathcal{O}(1/\Lambda^4)$ .

bounds from the electroweak precision data. This is due to the antisymmetry of the epsilon tensor which is present in all CP-odd operators. In fact, because of the same reason, all quantum corrections to gauge boson two-point functions up to  $\mathcal{O}(\frac{1}{\Lambda^2})$  vanish<sup>2</sup> and first nonzero contributions due to CP-odd operators appear at  $\mathcal{O}(\frac{1}{\Lambda^4})$ . As we will see in section 4, the CP-odd couplings contribute to observables related to LHC Higgs data at this order. It would be interesting to discuss the implications of the electroweak precision measurement constraints on the parameters of CP-odd operators.

It is well known that the dominant effects of new physics can be conveniently parametrized in terms of Peskin-Takeuchi parameters [60]. These are related to the gauge boson two-point functions as,

$$\alpha S = 4c_W^2 s_W^2 \left( \Pi'_{ZZ}(0) - \Pi'_{\gamma\gamma}(0) - \frac{c_W^2 - s_W^2}{s_W c_W} \Pi'_{\gamma Z}(0) \right) \quad (12)$$

$$\alpha T = \frac{\Pi_{WW}(0)}{m_W^2} - \frac{\Pi_{ZZ}(0)}{m_Z^2} \quad (13)$$

$$\alpha U = 4s_W^2 \left( \Pi'_{WW}(0) - c_W \Pi'_{ZZ}(0) - s_W^2 \Pi'_{\gamma\gamma}(0) - 2c_W s_W \Pi'_{\gamma Z}(0) \right) \quad (14)$$

where,  $\Pi_{V_1 V_2}(p^2)$  and  $\Pi'_{V_1 V_2}(p^2)$  are the  $g^{\mu\nu}$  part of the two-point function and its derivative with respect to  $p^2$ , respectively. The relevant one-loop Feynman diagrams are shown in Fig. 1. We have regularized ultraviolet (UV) singularities of these diagrams in dimensional regularization (DR). The expressions for  $\Pi_{V_1 V_2}(p^2)$  in terms of standard one-loop scalar functions are given in Appendix A. We find that  $\Pi_{\gamma\gamma}(0) = \Pi_{\gamma Z}(0) = 0$  which is expected due to the transverse nature of the photon. The renormalization of UV singularity is carried out in  $\overline{\text{MS}}$  scheme which introduces scale dependence in these expressions. We have identified the renormalization scale with the cutoff scale  $\Lambda$ . Thus the gauge boson two-point functions also have  $\ln(\Lambda)$  dependence apart from the overall  $1/\Lambda^4$  dependence coming from CP-odd couplings. Because of this an explicit choice of  $\Lambda$  is necessary in deriving the EWP constraints on  $\tilde{f}_i$ s.

<sup>2</sup>These corrections are proportional to  $\epsilon^{\mu\nu\alpha\beta} p_\alpha p_\beta$  ( $p$  being the four-momentum of gauge boson) which is zero.

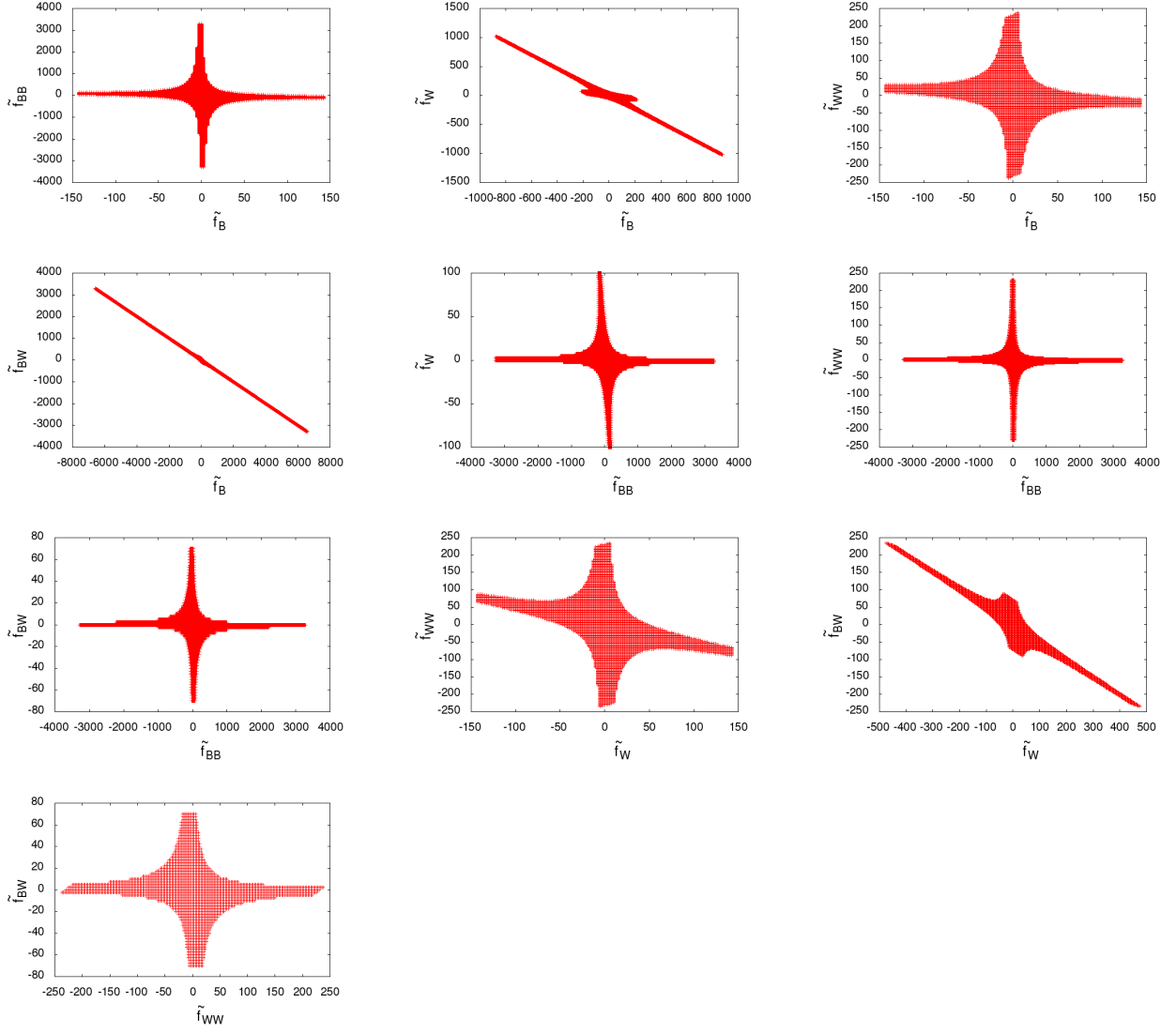


Figure 2: Constraints from electroweak precision data keeping two parameters nonzero at a time and for  $\Lambda = 1$  TeV.

For  $\Lambda = 1$  TeV, the Peskin-Takeuchi parameters due to CP-odd couplings are given by,

$$S = (-3.36 C_{\gamma\gamma h}^2 - 1.28 C_{\gamma Zh}^2 + 4.64 C_{ZZh}^2 - 4.49 C_{\gamma\gamma h} C_{\gamma Zh} - 6.21 C_{\gamma Zh} C_{ZZh}) \times 10^{-5} \quad (15)$$

$$T = -9.74 \times 10^{-5} C_{WW\gamma}^2 \quad (16)$$

$$U = (-0.960 C_{\gamma\gamma h}^2 - 4.69 C_{\gamma Zh}^2 - 4.64 C_{ZZh}^2 + 5.67 C_{WWh}^2 + 2.76 C_{WW\gamma}^2 - 3.59 C_{\gamma\gamma h} C_{\gamma Zh} - 4.96 C_{\gamma Zh} C_{ZZh}) \times 10^{-5}. \quad (17)$$

We can also express them in terms of  $\tilde{f}_i$ s using their relation with  $C_i$ s given in Table 1. The experimental limits on  $S, T$  and  $U$  parameters are obtained by fitting the data on various electroweak observables with these parameters. The limits are [50],

$$S = -0.03 \pm 0.10, \quad T = 0.01 \pm 0.12, \quad U = 0.05 \pm 0.10. \quad (18)$$

In Eqs. (15), (16) and (17) the coefficients of various couplings are  $\sim 10^{-5}$  suggesting that the EWP constraints cannot be very strong. Therefore, we only consider the case where any two out of five parameters are nonzero. In Fig. 2, we display the allowed range for CP-odd parameters which satisfy the above limits on  $S, T$  and  $U$  parameters for all ten sets of two parameters taken together. Here we have varied parameters freely to ensure that we obtain a bounded region. We note that large values of  $\mathcal{O}(1000)$  for  $\tilde{f}_{BB}$  are always allowed. On the other hand the allowed range for  $\tilde{f}_{WW}$  never goes beyond 250. Allowed values for all other parameters can be of  $\mathcal{O}(100 - 1000)$ . Some of these observations can be understood once we express the  $S, T$  and  $U$  parameters in terms of  $\tilde{f}_i$ s. As we turn on other parameters, these constraints become weaker. Also, for a larger cutoff scale the allowed parameter space grows as one would expect.

## 4 Constraints from LHC data

The presence of CP-odd operators introduces modifications in the strength of the gauge-Higgs couplings, and hence changes the Higgs production and decay rates in channels involving these couplings. Since we are interested in CP-even observables, the SM  $VVh$  couplings which are CP-even, do not interfere with the CP-odd  $VVh$  couplings. Hence the lowest order (tree level) modifications to the decay widths ( $\Gamma$ ) and production cross sections ( $\sigma$ ) are of the order  $\frac{1}{\Lambda^4}$ . To quantify these changes we define the following ratios for various decay and production channels,

$$\alpha_Y = \frac{\Gamma^{\text{BSM}}(h \rightarrow Y)}{\Gamma^{\text{SM}}(h \rightarrow Y)} \quad (19)$$

$$\gamma_X = \frac{\sigma^{\text{BSM}}(X \rightarrow h)}{\sigma^{\text{SM}}(X \rightarrow h)} \quad (20)$$

where  $Y$  and  $X$  are used to label the final state and initial state particles in the Higgs decay and production channels respectively.

### 4.1 Higgs decay channels

In the SM, the 126 GeV Higgs boson predominantly decays into  $b\bar{b}$  and  $WW^*$  followed by  $gg$ ,  $\tau^+\tau^-$ ,  $c\bar{c}$  and  $ZZ^*$ . It also decays to  $\gamma\gamma$ ,  $\gamma Z$  and  $\mu^+\mu^-$  with much suppressed rates. Out of these,  $h \rightarrow gg$ ,  $h \rightarrow \gamma\gamma$  and  $h \rightarrow \gamma Z$  are loop-induced decay modes and hence are sensitive to new physics. The decay channels which are affected by the CP-odd operators are  $h \rightarrow \gamma\gamma$ ,  $h \rightarrow \gamma Z$ ,  $h \rightarrow WW^*$  and



$h \rightarrow ZZ^*$ . The expressions for the ratio of the decay widths,  $\alpha_{ij}$  in various two body Higgs decay channels are as follows <sup>3</sup>:

$$\alpha_{\gamma\gamma} = 1 + 2.84 \left( \frac{C_{\gamma\gamma h}^2}{\Lambda^4} \right) \quad (22)$$

$$\alpha_{\gamma Z} = 1 + 0.856 \left( \frac{C_{\gamma Zh}^2}{\Lambda^4} \right) \quad (23)$$

$$\alpha_{WW^*} = 1 + 3.35 \times 10^{-6} \left( \frac{C_{WWh}^2}{\Lambda^4} \right) \quad (24)$$

$$\alpha_{2\ell 2\nu} = 1 + 3.56 \times 10^{-6} \left( \frac{C_{WWh}^2}{\Lambda^4} \right) \quad (25)$$

$$\alpha_{ZZ^*} = 1 + 1.40 \times 10^{-6} \left( \frac{C_{ZZh}^2}{\Lambda^4} \right) \quad (26)$$

$$\alpha_{4\ell} = 1 + 1.54 \times 10^{-6} \left( \frac{C_{ZZh}^2}{\Lambda^4} \right) \quad (27)$$

Since the set of gauge-Higgs operators considered in our analysis do not alter the Higgs coupling with gluons ( $g$ ) and fermions ( $f$ ), we have  $\alpha_{ff} = \alpha_{gg} = 1$ . The ratios  $\alpha_{2\ell 2\nu}$  [Eq.( 25)] and  $\alpha_{4\ell}$  [Eq.( 27)] correspond to the  $h \rightarrow WW^* \rightarrow 2\ell 2\nu$  and  $h \rightarrow ZZ^* \rightarrow 4\ell$  respectively. Here  $\ell$  stands for electron and muon, and  $\nu$  for corresponding neutrinos. The ratios  $\alpha_{WW^*}$  and  $\alpha_{ZZ^*}$  which include both leptonic and hadronic decays of  $W$  and  $Z$  bosons are used in calculating modified total Higgs decay width. As mentioned earlier, the modifications to Higgs partial decay widths at leading order are  $\mathcal{O}(1/\Lambda^4)$ . It is in contrast to the case of CP-even dimension six gauge-Higgs operators where such modifications occur at  $\mathcal{O}(1/\Lambda^2)$ . Unlike  $WWh$  and  $ZZh$  couplings, the  $\gamma\gamma h$  and  $\gamma Zh$  couplings are loop-induced in the SM. In the presence of CP-odd operators these vertices receive contributions at tree level. This explains the relatively large coefficients in the expressions for  $\alpha_{\gamma\gamma}$  [Eq.( 22)] and  $\alpha_{\gamma Z}$  [Eq.( 23)] as compared to the other decay width ratios. This would imply most stringent constraints on the parameters contributing to these decay channels. For further discussion on CP-odd vs. CP-even operators, we refer the reader to section 6.

## 4.2 Higgs production channels

At the LHC, the dominant mode to produce Higgs boson is gluon-gluon fusion (GGF) mediated by a top quark loop. The other major production channels include: vector boson fusion (VBF), associated production with a weak boson ( $Vh$ ) and associated production with a pair of top quark ( $t\bar{t}h$ ). Except GGF and  $t\bar{t}h$  production channels, all other channels are affected in presence of anomalous gauge-Higgs CP-odd vertices. Like the decay width ratios, the production cross section ratios also receive modifications at  $\mathcal{O}(1/\Lambda^4)$ . The ratios of the Higgs production cross sections,  $\gamma_X$  in various channels at  $\sqrt{S} = 8(7)$  TeV LHC are given below.

<sup>3</sup> We disagree with the CP-odd part of the analytic expression for  $\alpha_{\gamma Z}$  in Eq. (3.17) of Ref. [45]. The correct expression for CP-odd term in the notations of Ref. [45] turns out to be,

$$\alpha_{\gamma Z} = 1 + \left| \frac{4\sqrt{2}\pi^2 \tilde{a}_2}{G_F \Lambda^2 s_W^2 (A_F + A_W)} \right|^2, \quad (21)$$

where  $\tilde{a}_2$  can be identified with the factor  $\frac{1}{2}C_{\gamma Zh}$  in our notation.

$$\gamma_{pp \rightarrow Wh} = 1 + 5.61(5.37) \times 10^{-4} \left( \frac{C_{WWWh}^2}{\Lambda^4} \right) \quad (28)$$

$$\gamma_{pp \rightarrow Wh \rightarrow h\nu} = 1 + 5.67(5.16) \times 10^{-4} \left( \frac{C_{WWWh}^2}{\Lambda^4} \right) \quad (29)$$

$$\begin{aligned} \gamma_{pp \rightarrow Zh} &= 1 + 4.09(3.92) \times 10^{-4} \left( \frac{C_{ZZZh}^2}{\Lambda^4} \right) + 2.45(2.32) \times 10^{-4} \left( \frac{C_{\gamma Zh}^2}{\Lambda^4} \right) \\ &\quad + 2.55(2.44) \times 10^{-4} \left( \frac{C_{ZZZh}}{\Lambda^2} \right) \left( \frac{C_{\gamma Zh}}{\Lambda^2} \right) \end{aligned} \quad (30)$$

$$\begin{aligned} \gamma_{\text{VBF}} &= 1 + 7.02(5.62) \times 10^{-6} \left( \frac{\tilde{f}_B^2}{\Lambda^4} \right) + 1.50(1.44) \times 10^{-4} \left( \frac{\tilde{f}_W^2}{\Lambda^4} \right) + 1.84(1.80) \times 10^{-5} \left( \frac{\tilde{f}_{BB}^2}{\Lambda^4} \right) \\ &\quad + 6.98(6.75) \times 10^{-4} \left( \frac{\tilde{f}_{WW}^2}{\Lambda^4} \right) + 4.39(4.38) \times 10^{-5} \left( \frac{\tilde{f}_{BW}^2}{\Lambda^4} \right) - 1.32(1.14) \times 10^{-5} \left( \frac{\tilde{f}_B \tilde{f}_W}{\Lambda^4} \right) \\ &\quad + 8.96(22.2) \times 10^{-7} \left( \frac{\tilde{f}_B \tilde{f}_{BB}}{\Lambda^4} \right) - 5.06(5.03) \times 10^{-5} \left( \frac{\tilde{f}_B \tilde{f}_{WW}}{\Lambda^4} \right) \\ &\quad + 2.63(2.59) \times 10^{-5} \left( \frac{\tilde{f}_B \tilde{f}_{BW}}{\Lambda^4} \right) + 8.98(9.21) \times 10^{-7} \left( \frac{\tilde{f}_W \tilde{f}_{BB}}{\Lambda^4} \right) \\ &\quad + 6.22(5.98) \times 10^{-4} \left( \frac{\tilde{f}_W \tilde{f}_{WW}}{\Lambda^4} \right) - 2.46(2.71) \times 10^{-5} \left( \frac{\tilde{f}_W \tilde{f}_{BW}}{\Lambda^4} \right) \\ &\quad - 3.51(3.60) \times 10^{-5} \left( \frac{\tilde{f}_{BB} \tilde{f}_{BW}}{\Lambda^4} \right) + 3.27(3.85) \times 10^{-5} \left( \frac{\tilde{f}_{BB} \tilde{f}_{WW}}{\Lambda^4} \right) \\ &\quad - 1.43(1.45) \times 10^{-4} \left( \frac{\tilde{f}_{WW} \tilde{f}_{BW}}{\Lambda^4} \right) \end{aligned} \quad (31)$$

$$\gamma_{pp \rightarrow tth} = \gamma_{\text{GGF}} = 1. \quad (32)$$

These expressions have been obtained by computing the SM and BSM cross sections at tree level using **Madgraph** [61] under the assumption that the K-factors (due to higher order corrections) are same in the SM and BSM cases. For that we have implemented our effective Lagrangian in **FeynRules** [62] and used the generated UFO model file in **Madgraph**. The cross sections have been calculated using **cteq611** parton distribution functions [63] and with default settings for renormalization and factorization scales.

We would like to point out that there is an additional diagram which contributes to  $pp \rightarrow Zh$  due to tree level CP-odd  $\gamma Zh$  coupling. Similarly, in VBF channel additional diagrams appear due to both  $\gamma\gamma h$  and  $\gamma Zh$  couplings. Because of a different parametrization, this information is not explicit in the expression for VBF. We find this parametrization more convenient in terms of evaluating the coefficients in Eq.( 31). Also, the VBF coefficients reported above do not have any  $Vh$  contamination and this can be ensured in **Madgraph** at the process generation level. One can notice that the modifications induced by the CP-odd operators are relatively weak because the SM cross sections are already tree level effects in the modified production channels.

One important fact in relation to these production cross section ratios ( $\gamma$ s) is that the numerical coefficients present in these expressions are very much cut dependent. This is associated with the fact that the anomalous couplings induced by the gauge-Higgs operators have a different Lorentz structure (therefore, different kinematic dependence) than their SM counterparts. Hence in general

Production channel	8 TeV cross section (pb)	7 TeV cross section (pb)
$GGF$	18.97	14.89
$VBF$	1.568	1.211
$Wh$	0.686	0.563
$Zh$	0.405	0.327
$t\bar{t}h$	0.1262	0.0843
$b\bar{b}h$	0.198	0.152

Table 2: Higgs production cross section in the SM [64].

the SM and BSM cut efficiencies are not the same for a given process. The differences between the two become more pronounced for higher values of the CP-odd couplings. But for reasonably low values of the same one can still work under the approximation that the two cut efficiencies are the same. In this work we have taken this approximation into consideration, and taken only default cuts in **Madgraph** to simulate any production or decay channel. Since we have taken data only from individual production channels and not from combined channel data (e.g.  $Vh$  combined channel) in our chi-square analysis, this approximation finds a stronger footing.

### 4.3 Global analysis

The quantitative measure of the difference between the Higgs data from the LHC, and its corresponding SM predictions is given by what we call the signal strength, defined as,

$$\mu^{X,Y} = \frac{\sigma^{\text{BSM}}(X \rightarrow h) \text{BR}^{\text{BSM}}(h \rightarrow Y)}{\sigma^{\text{SM}}(X \rightarrow h) \text{BR}^{\text{SM}}(h \rightarrow Y)} \quad (33)$$

where,  $\text{BR}(h \rightarrow Y) = \frac{\Gamma(h \rightarrow Y)}{\Gamma_{\text{total}}}$  is the branching ratio for Higgs decaying into  $Y$  final state, and  $\Gamma_{\text{total}}$  is the total Higgs decay width. For 126 GeV Higgs boson  $\Gamma_{\text{total}}^{\text{SM}} = 4.2$  MeV. The total Higgs decay width in the BSM construct  $\Gamma_{\text{total}}^{\text{BSM}}$  can be expressed in terms of the SM total Higgs decay width  $\Gamma_{\text{total}}^{\text{SM}}$  by,

$$\Gamma_{\text{total}}^{\text{BSM}} = S_{\text{total}} \Gamma_{\text{total}}^{\text{SM}}. \quad (34)$$

$S_{total}$  is given in terms of the various branching fractions of the Higgs in the SM as,

$$S_{total} \sim \text{BR}_{bb}^{\text{SM}} + \text{BR}_{cc}^{\text{SM}} + \text{BR}_{\tau\tau}^{\text{SM}} + \alpha_{\gamma\gamma} \text{BR}_{\gamma\gamma}^{\text{SM}} + \alpha_{\gamma Z} \text{BR}_{\gamma Z}^{\text{SM}} \\ + \alpha_{WW^*} \text{BR}_{WW^*}^{\text{SM}} + \alpha_{ZZ^*} \text{BR}_{ZZ^*}^{\text{SM}} + \alpha_{gg} \text{BR}_{gg}^{\text{SM}} \quad (35)$$

which becomes on solving,

$$S_{total} \sim 0.736 + 0.0023\alpha_{\gamma\gamma} + 0.0016\alpha_{\gamma Z} + 0.23\alpha_{WW^*} + 0.029\alpha_{ZZ^*}. \quad (36)$$

The SM branching fractions for 126 GeV Higgs are taken from [64]. The signal strength in Eq.( 33) can be rewritten in a compact form using the decay and the productions cross section ratios defined above,

$$\mu^{X,Y} = \gamma_X \frac{\alpha_Y}{S_{total}}. \quad (37)$$

To perform the global fit of our CP-odd parameters, we use the standard definition of the chi-square function,

$$\chi^2 = \sum_{X,Y} \frac{(\mu_{th}^{X,Y} - \mu_{exp}^{X,Y})^2}{\Sigma_{X,Y}^2} \quad (38)$$

where  $\mu_{th}^{X,Y}$  is the theoretical signal strength expected in presence of CP-odd operators, and  $\mu_{exp}^{X,Y}$  is the experimental signal strength reported by the LHC experiments.  $\Sigma_{X,Y}$  is the experimental uncertainty in  $\mu_{exp}^{X,Y}$ . The experimental data reported generally has unsymmetrical uncertainties  $\Sigma_{X,Y}^+$  and  $\Sigma_{X,Y}^-$ . The  $\Sigma_{X,Y}$  that we use symmetrizes these uncertainties through the following definition,

$$\Sigma_{X,Y} = \sqrt{\frac{(\Sigma_{X,Y}^+)^2 + (\Sigma_{X,Y}^-)^2}{2}}. \quad (39)$$

Since the LHC data that we use includes data from both 7 and 8 TeV LHC runs, the theoretical signal strength in Eq.( 38) is obtained after combining the signal strengths calculated for 7 and 8 TeV LHC. For that we have used following formula [43],

$$\mu_{th}^{XY} = \frac{\mu_{th,8}^{XY} \sigma_8^{\text{SM}} \mathcal{L}_8 + \mu_{th,7}^{XY} \sigma_7^{\text{SM}} \mathcal{L}_7}{\sigma_8^{\text{SM}} \mathcal{L}_8 + \sigma_7^{\text{SM}} \mathcal{L}_7} \quad (40)$$

where  $\mathcal{L}_7$  and  $\mathcal{L}_8$  are the luminosities at 7 and 8 TeV, respectively, and  $\sigma_7^{\text{SM}}$  and  $\sigma_8^{\text{SM}}$  are the SM cross sections at those energies. These cross sections are listed in Table 2.

In our analysis we have taken total 15 data points which are the most updated ones. We have listed them in Table 3. Note that due to large uncertainty we do not include Higgs data in  $h \rightarrow \gamma Z$  decay channel [65, 66] from CMS and ATLAS. The global analysis with five CP-odd parameters results into  $\chi_{min}^2 = 6.78$ . However, in this case the best fit point is very unstable with respect to the step size that we choose to scan the parameter space. Also, we find that the  $\chi_{min}^2$  is insensitive to the parameters  $\tilde{f}_B$  and  $\tilde{f}_W$ . These are the parameters which do not enter the  $\gamma\gamma h$  vertex and their coefficients are very small compared to those of  $\tilde{f}_{BB}$ ,  $\tilde{f}_{WW}$  and  $\tilde{f}_{BW}$ , which do enter the  $\gamma\gamma h$  vertex [Eq.( 22)]. Since the LHC observables have an overall cutoff scale dependence, the ratio  $\tilde{f}_i/\Lambda^2$  can be taken as the effective parameter to be constrained. In other words, the constraints from global analysis can be easily predicted for any value of  $\Lambda$  of interest.

We organize the constraints on CP-odd parameters from global fit of LHC data in the following two parts.

Production channel	Decay channel	Signal strength	Energy in TeV (Luminosity in $fb^{-1}$ )
GGF (ATLAS)	$h \rightarrow \gamma\gamma$	$1.32 \pm 0.38$ [67]	7(4.5) + 8(20.3)
VBF (ATLAS)	$h \rightarrow \gamma\gamma$	$0.8 \pm 0.7$ [67]	7(4.5) + 8(20.3)
$Wh$ (ATLAS)	$h \rightarrow \gamma\gamma$	$1.0 \pm 1.6$ [67]	7(4.5) + 8(20.3)
$Zh$ (ATLAS)	$h \rightarrow \gamma\gamma$	$0.1^{+3.7}_{-0.1}$ [67]	7(4.5) + 8(20.3)
$t\bar{t}h$ (ATLAS)	$h \rightarrow \gamma\gamma$	$1.6^{+2.7}_{-1.8}$ [67]	7(4.5) + 8(20.3)
GGF (CMS)	$h \rightarrow \gamma\gamma$	$1.12^{+0.37}_{-0.32}$ [68]	7(5.1) + 8(19.7)
VBF (CMS)	$h \rightarrow \gamma\gamma$	$1.58^{+0.77}_{-0.68}$ [68]	7(5.1) + 8(19.7)
$t\bar{t}h$ (CMS)	$h \rightarrow \gamma\gamma$	$2.69^{+2.51}_{-1.81}$ [68]	7(5.1) + 8(19.7)
GGF + $t\bar{t}h$ + $b\bar{b}h$ (ATLAS)	$h \rightarrow ZZ^* \rightarrow 4\ell$	$1.7^{+0.5}_{-0.4}$ [69]	7(4.5) + 8(20.3)
GGF + $t\bar{t}h$ (CMS)	$h \rightarrow ZZ^* \rightarrow 4\ell$	$0.8^{+0.46}_{-0.36}$ [70]	7(5.1) + 8 (19.7)
GGF (ATLAS)	$h \rightarrow WW^* \rightarrow 2\ell 2\nu$	$1.01^{+0.27}_{-0.25}$ [71]	7(4.5) + 8(20.3)
VBF (ATLAS)	$h \rightarrow WW^* \rightarrow 2\ell 2\nu$	$1.28^{+0.53}_{-0.45}$ [71]	7(4.5) + 8(20.3)
GGF (CMS)	$h \rightarrow WW^* \rightarrow 2\ell 2\nu$	$0.74^{+0.22}_{-0.20}$ [72]	7(4.9) + 8 (19.4)
VBF (CMS)	$h \rightarrow WW^* \rightarrow 2\ell 2\nu$	$0.6^{+0.57}_{-0.46}$ [72]	7(4.9) + 8 (19.4)
$Wh \rightarrow h\ell\nu$ (CMS)	$h \rightarrow WW^* \rightarrow 2\ell 2\nu$	$0.56^{+1.27}_{-0.95}$ [72]	7(4.9) + 8 (19.4)

Table 3: LHC data used in the global analysis.

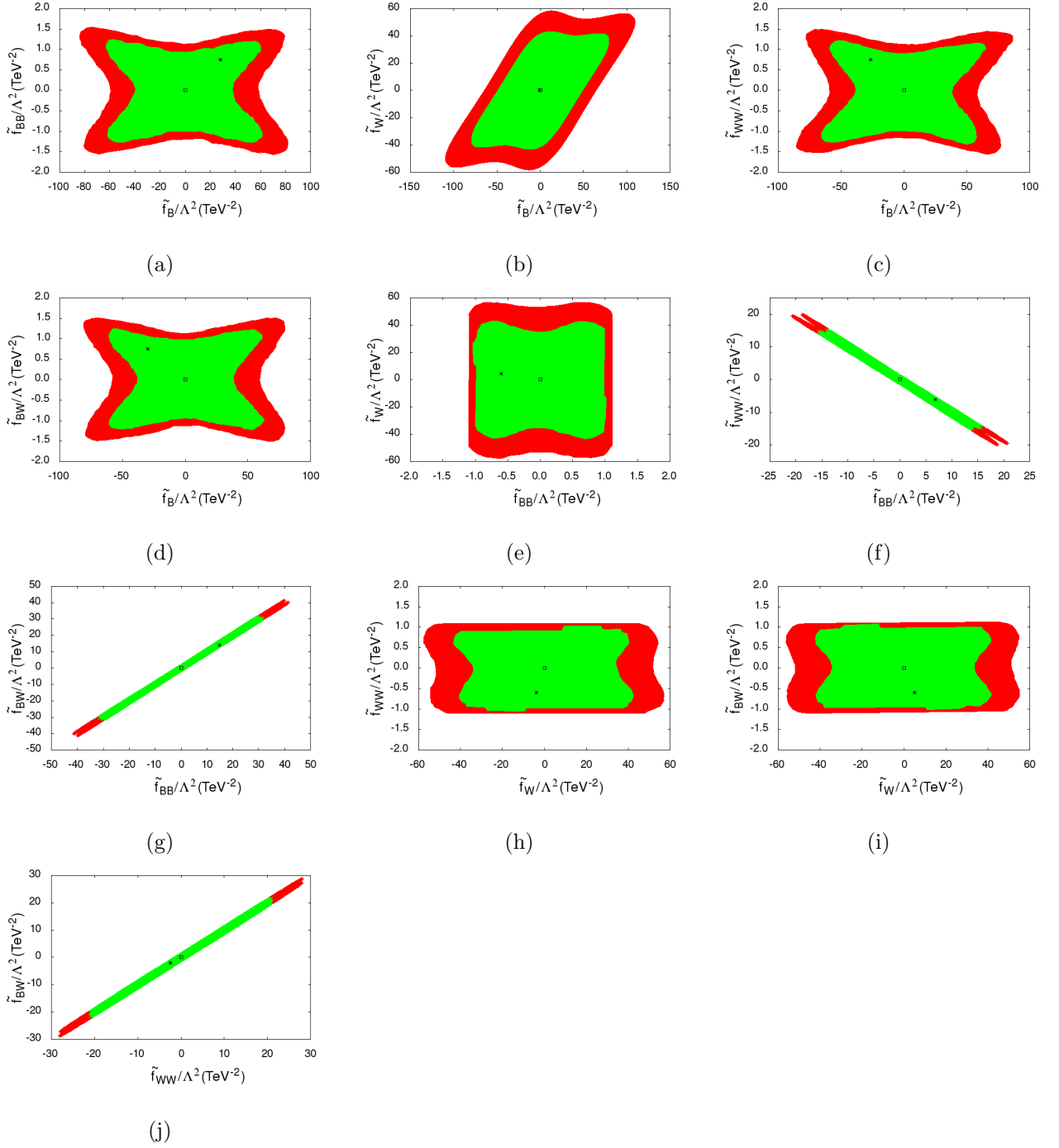


Figure 3: Global fits of the CP-odd parameters keeping two parameters nonzero at a time. The point (0,0) corresponds to the SM point and the (\*) represents the best fit point. The green region corresponds to the 68 percent confidence interval and the red region to the 95 percent confidence interval, respectively. The best fit point is doubly degenerate up to a sign flip of the best fit point coordinates.

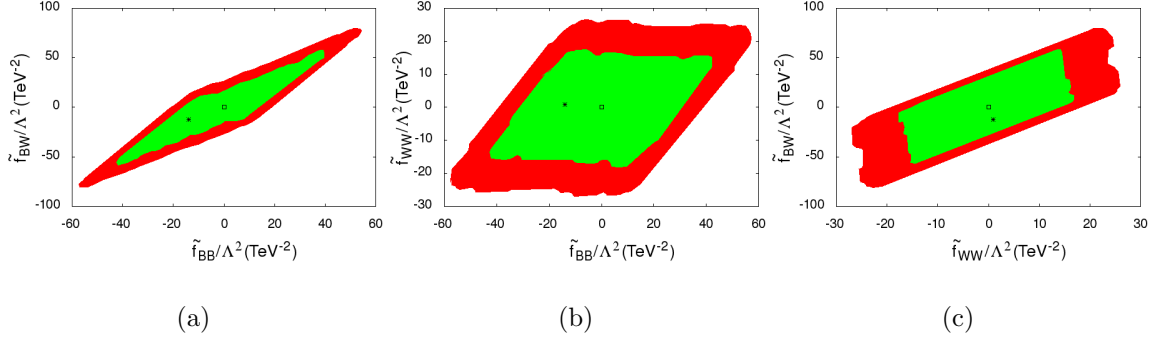


Figure 4: Marginalized global fits of the CP-odd parameters with  $\tilde{f}_W = \tilde{f}_B = 0$ .

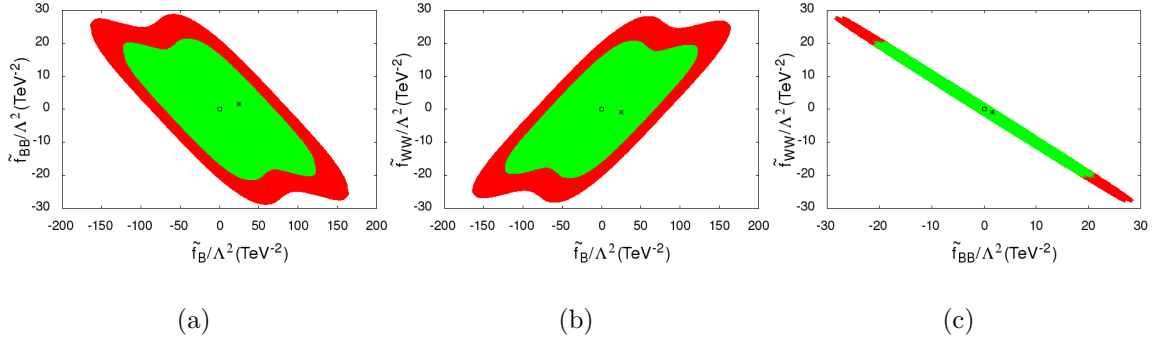


Figure 5: Marginalized global fits of the CP-odd parameters with  $\tilde{f}_W = \tilde{f}_{BW} = 0$ .

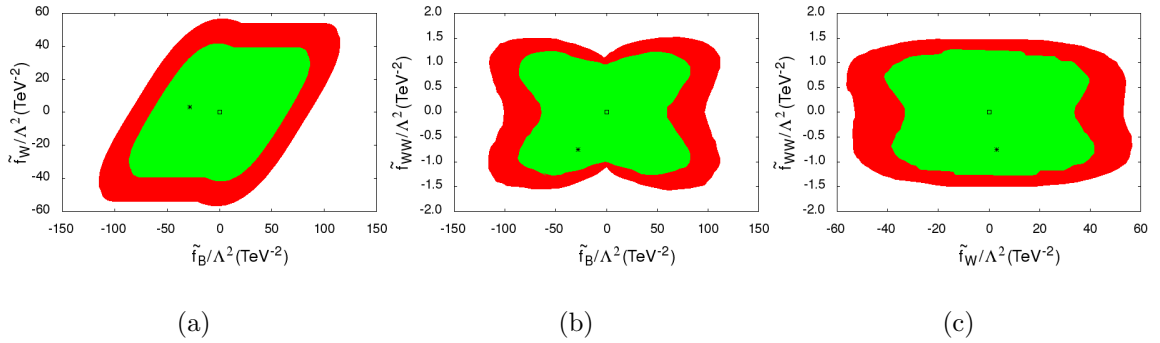


Figure 6: Marginalized global fits of the CP-odd parameters with  $\tilde{f}_{BB} = \tilde{f}_{BW} = 0$ .

- We have five CP-odd parameters ( $\tilde{f}_W, \tilde{f}_B, \tilde{f}_{BB}, \tilde{f}_{BW}, \tilde{f}_{WW}$ ) and in the first case we consider any two of them to be non-zero and put limits on them. There are a total of ten such combinations. The allowed parameter space with 68% and 95% confidence levels are shown in Fig.3. In generating these plots we have varied parameters freely. Even if one considers the perturbativity argument, the tightest upper bound on these CP-odd parameters is of the order  $\sim 100$ . We can see that in all cases the allowed parameter space is bounded. The parameters which enter the  $\gamma\gamma h$  vertex ( $\gamma\gamma h$  family) *i.e.*,  $\tilde{f}_{BB}, \tilde{f}_{WW}$  and  $\tilde{f}_{BW}$  are in general more constrained than those which do not enter the  $\gamma\gamma h$  vertex (non- $\gamma\gamma h$  family) *i.e.*,  $\tilde{f}_B$  and  $\tilde{f}_W$ . When any of the three  $\gamma\gamma h$  parameters is taken together with  $\tilde{f}_B$  or  $\tilde{f}_W$  as shown in Figs 3a,3c,3d,3e, 3h and 3i, we find that it is much tightly constrained and allowed values are of  $\mathcal{O}(1)$ . However, among themselves these parameters are highly correlated and cancellation among them leads to larger allowed values of  $\mathcal{O}(10)$  (see Figs. 3f,3g and 3j). The nature of slope in these figures is related to the relative sign among  $\tilde{f}_{BB}, \tilde{f}_{WW}$  and  $\tilde{f}_{BW}$ . We also note that out of  $\tilde{f}_B$  and  $\tilde{f}_W$ ,  $\tilde{f}_W$  is always more constrained. For example, the maximum allowed value for  $\tilde{f}_B$  is  $\sim 100$  while the allowed values of  $\tilde{f}_W$  are less than 60, see Fig. 3b. This observation can be attributed to the relative size of their coefficients in various observables. We have also found that the inclination of the plot in Fig. 3b is governed by the  $C_{\gamma Zh}$  which enters  $Zh$  and VBF production channels and affects the  $S_{total}$  [Eq.( 36)].
- In the second case we consider three parameters at a time in the global analyses. Once again there are ten such combinations. Following the general conclusions of two-parameter case, we can categorize these combinations into three groups. This categorization is based on the number of parameters from the  $\gamma\gamma h$  family being present in each combination. Thus we have one combination where all the parameters are from  $\gamma\gamma h$  family (G1), six combinations where two parameters are from  $\gamma\gamma h$  family and one from non- $\gamma\gamma h$  family (G2) and three combinations where one is from  $\gamma\gamma h$  family and the other two are  $\tilde{f}_B$  and  $\tilde{f}_W$  (G3). We present results for three representative combinations (one from each group): (i)  $\{ \tilde{f}_{BB}, \tilde{f}_{WW}, \tilde{f}_{BW} \}$ ; (ii)  $\{ \tilde{f}_{BB}, \tilde{f}_{WW}, \tilde{f}_B \}$ ; (iii)  $\{ \tilde{f}_{WW}, \tilde{f}_B, \tilde{f}_W \}$ . The allowed parameter space for these combinations are shown in Figs. 4, 5 and 6, respectively. The two-parameter plots here are obtained after marginalizing over the third parameter.

As compared to two-parameter plots (see Fig. 3), the allowed region here is more diffused due to the presence of the third parameter. This is particularly noticeable for the first set of plots in Fig. 4. We find that  $\tilde{f}_{WW}$  being present in all  $VVh$  couplings gets stronger bounds, while  $\tilde{f}_{BW}$  is least constrained in set (i). From the plots of Fig. 5 which belong to set (ii) we can infer that the parameters of  $\gamma\gamma h$  family are more constrained. However, mutual cancellation still allows values of  $\mathcal{O}(30)$  for them. The opposite inclinations of the plots in 5a and 5b can be related to how  $\tilde{f}_{BB}$  and  $\tilde{f}_{WW}$  enter in  $\gamma\gamma h$  vertex to maintain cancellation and it is confirmed by the nature of the slope in Fig. 5c. Note that Fig. 5c is very much similar to the corresponding plot in Fig. 3f. This is expected because the global analysis is not very sensitive to  $\tilde{f}_B$ . Interestingly, the parameter sets  $\{ \tilde{f}_{WW}, \tilde{f}_{BW}, \tilde{f}_W \}$  and  $\{ \tilde{f}_{BB}, \tilde{f}_{BW}, \tilde{f}_B \}$  which would also belong to group G2 are less constrained. We find that the parameter regions are still bounded but boundary values for  $\tilde{f}_W$  and  $\tilde{f}_B$  in these sets are about 800 and 2500, respectively. For the parameters in set (iii) we can conclude that  $\tilde{f}_{WW}$  being the only parameter present from the  $\gamma\gamma h$  family is very tightly constrained as shown by the plots in Figs. 6b and 6c.

We have also checked that the constraints on CP-odd parameters from the direct and indirect measurements of the Higgs total width [70, 73] are weaker than those obtained from the global analysis. On the whole,  $\tilde{f}_{BB}, \tilde{f}_{WW}$  and  $\tilde{f}_{BW}$  contribute to the  $\gamma\gamma h$  vertex at tree level and thus



are constrained rather tightly compared to  $\tilde{f}_B$  and  $\tilde{f}_W$ . The fact that one has SM contribution at the one-loop level only is responsible for this.  $\tilde{f}_B$  and  $\tilde{f}_W$  are relatively loosely constrained due to the lack of sufficient data on the channel  $h \rightarrow \gamma Z$ , to which they contribute.

The constraints on the parameter space of our CP-violating operators, as obtained from global fits of the (7 + 8) TeV data, are expected to be improved in the high energy runs. A tentative estimate of such improvements, as also that in a linear  $e^+e^-$  collider, can be found, for example, in [74]. Going by the estimates of [74], the uncertainty in the signal strength measurements in the next run can be reduced to 33% of the present uncertainties as obtained by both ATLAS and CMS for the  $\gamma\gamma$  and  $WW^*$  final states in the gluon fusion channel. A precise answer on the improvement of our limits, however, depends also on any possible shift in the central values of the measured signal strengths in different channels. This in turn is also a function of the various systematic uncertainties in the new run, and therefore we have to wait for more data before some precise conclusions can be drawn. A similar consideration applies to a linear collider; precision in coupling measurements down to 1% is expected there in principle [74], but the available statistics as well as the systematics need to be known before concrete estimates emerge.

## 5 Constraints from EDMs

The fermionic electric dipole moment receive an additional contribution from these new CP-odd higher-dimensional operators involving Higgs and pair of gauge bosons. Nonobservation of any fermionic EDMs puts severe constraints on the parameters  $\tilde{f}_i$ s. The fermion EDM operator is defined as,

$$-\frac{1}{2} d_f \bar{\psi}(p_2) i\gamma^5 \sigma^{\mu\nu} \psi(p_1) F_{\mu\nu}, \quad (41)$$

where,  $\sigma^{\mu\nu} = \frac{i}{2}[\gamma^\mu, \gamma^\nu]$  and  $d_f$  is known as the fermion EDM form factor. Nonvanishing EDMs provide clear hint of CP-violation [75, 76]. In the standard model, CP violation occurs due to quark mixing and it is quite weak (1 part in 1000) [50]. On top of that the first nonzero contribution to EDM operator in the SM appears at three loop level in quark sector, while, for leptons it arises at four loop level. The present upper limits on electron and neutron EDMs are much larger than the values predicted by the SM [77]. In presence of CP-odd gauge-Higgs operators  $\gamma\gamma h$ ,  $\gamma Zh$  and  $WW\gamma$  couplings are modified, because of which the leading contribution to fermion EDMs appears at one-loop level. Due to this the fermion EDM measurements can provide stringent bounds on the CP-odd parameters. Note that the contribution to the fermion EDMs from CP-odd  $WW h$  and  $ZZ h$  vertices can result only at two-loop level. Since the two-loop effects are expected to be subdominant, we will derive constraints on the CP-odd parameters from one-loop fermion EDM calculations. The diagrams that contribute to the fermion EDM at one-loop level are shown in Fig.7.

The expression for the fermion EDM form factor  $d_f$  at one-loop due to the  $\gamma\gamma h$ ,  $\gamma Zh$  and  $WW\gamma$  vertices is given by the following equation<sup>4</sup>:

$$d_f = \frac{m_f e \alpha}{\pi v^2} \left[ \tilde{a}_1 K_1(\Lambda, m_h) + \tilde{a}_2 K_2(\Lambda, m_Z, m_h) + \tilde{a}_3 K_1(\Lambda, m_W) \right] \quad (42)$$

where,

$$\tilde{a}_1 = -\frac{Q_f}{4s_W^2} C_{\gamma\gamma h}; \quad \tilde{a}_2 = \frac{\left(\frac{1}{2}I_f - Q_f s_W^2\right)}{t_W s_{2W}^2} C_{\gamma Zh}; \quad \tilde{a}_3 = -\frac{I_f}{4s_W^3} C_{WW\gamma}. \quad (43)$$

---

<sup>4</sup>We have observed a relative sign change in the contribution of the  $WW\gamma$  diagram to the EDM, for the  $u$  and  $d$  quarks, which is taken care of by the factor  $I_f$  in  $\tilde{a}_3$ . It was unaccounted by Ref. [45] where a similar calculation is done.

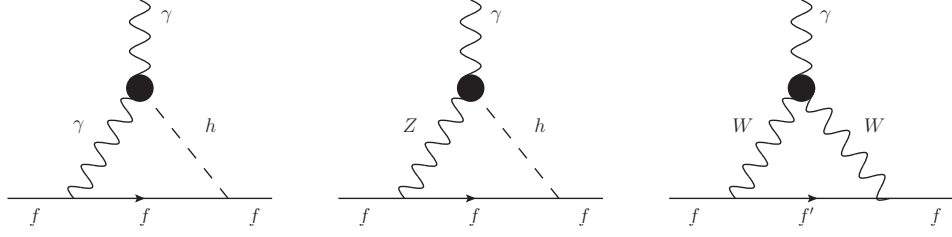


Figure 7: One-loop diagrams contributing to fermion EDMs. The blobs show the effective vertices arising out of the CP-odd operators.

Here,  $v$  is the electroweak symmetry breaking scale,  $\alpha$  is the fine structure constant,  $I_f$  is the third component of the fermion Isospin and  $Q_f$  is its electric charge quantum number. We have neglected the fermion masses ( $m_f$ ) with respect to other mass scales in the loop. The one-loop factors  $K_1$  and  $K_2$  are calculated in dimensional regularization ( $d = 4 - 2\epsilon$ ). Since these loops are UV divergent, we renormalize them in  $\overline{\text{MS}}$  scheme and identify the renormalization scale with the cutoff  $\Lambda$ . The expressions for  $K_1$  and  $K_2$  are given by,

$$K_1(\Lambda, x) = \frac{v^2}{\Lambda^2} \left[ \frac{1}{2} \ln \frac{\Lambda^2}{x^2} + \frac{3}{4} \right], \quad (44)$$

$$K_2(\Lambda, x, y) = \frac{v^2}{\Lambda^2} \left[ \frac{1}{2} \frac{x^2 \ln \frac{\Lambda^2}{x^2} - y^2 \ln \frac{\Lambda^2}{y^2}}{x^2 - y^2} + \frac{3}{4} \right]. \quad (45)$$

In the above, the finite factors of  $\frac{3}{4}$  are artifact of dimensional regularization. These factors do not appear in naive cutoff regularization.

The latest experimental bounds on the electron and neutron EDMs are [78–80],

$$\begin{aligned} |d_e| &< 8.7 \times 10^{-29} \text{ e cm} \\ |d_n| &< 2.9 \times 10^{-26} \text{ e cm.} \end{aligned} \quad (46)$$

Note that the EDM contribution is  $\mathcal{O}(\frac{1}{\Lambda^2})$  in the cutoff scale, therefore, it is expected to provide stronger bounds on CP-odd parameters than those obtained from EWP and LHC data. Like the electroweak precision observables calculated in section 3, the EDMs also have explicit dependence on  $\Lambda$ . Due to this, we provide EDM constraint equations for three different choices of cutoff scale  $\Lambda = 1, 5$  and 10 TeV.

- $\Lambda = 1 \text{ TeV}$

$$\begin{aligned} |d_e| &\equiv |233.86\tilde{f}_B + 260.45\tilde{f}_W - 390.92\tilde{f}_{BB} - 337.72\tilde{f}_{WW} + 858.63\tilde{f}_{BW}| < 1 \\ |d_n| &\equiv |7.02\tilde{f}_B + 13.81\tilde{f}_W - 8.91\tilde{f}_{BB} + 4.66\tilde{f}_{WW} + 22.96\tilde{f}_{BW}| < 1 \end{aligned} \quad (47)$$

- $\Lambda = 5 \text{ TeV}$

$$\begin{aligned} |d_e| &\equiv |13.87\tilde{f}_B + 15.63\tilde{f}_W - 24.60\tilde{f}_{BB} - 21.08\tilde{f}_{WW} + 52.34\tilde{f}_{BW}| < 1 \\ |d_n| &\equiv |0.40\tilde{f}_B + 0.85\tilde{f}_W - 0.57\tilde{f}_{BB} + 0.33\tilde{f}_{WW} + 1.36\tilde{f}_{BW}| < 1 \end{aligned} \quad (48)$$

- $\Lambda = 10 \text{ TeV}$

$$\begin{aligned} |d_e| &\equiv |3.95\tilde{f}_B + 4.47\tilde{f}_W - 7.11\tilde{f}_{BB} - 6.08\tilde{f}_{WW} + 15.02\tilde{f}_{BW}| < 1 \\ |d_n| &\equiv |0.11\tilde{f}_B + 0.24\tilde{f}_W - 0.16\tilde{f}_{BB} + 0.10\tilde{f}_{WW} + 0.39\tilde{f}_{BW}| < 1 \end{aligned} \quad (49)$$

The neutron EDM form factor ( $d_n$ ) is calculated in terms of constituent quark EDMs using the relation  $d_n = \frac{4}{3}d_d - \frac{1}{3}d_u$ , from the chiral-quark model [81]. In calculating the above constraints on the EDMs we take  $\alpha = 1/137$  and  $M_H = 126$  GeV. Because of a stronger experimental limit on electron EDM, the coefficients of parameters in  $d_e$  are larger than those in  $d_n$ . Our constraint equations for electron EDM form factor differ by an order of magnitude from those obtained in Ref. [45] mainly because we have used the most updated experimental bound on electron EDM [78].

We first consider the case when any two of the five parameters are kept nonzero. In this case, we freely vary the parameters. The constraints on the parameters are shown in Fig 8 for  $\Lambda = 1, 5$  and 10 TeV respectively. In all combinations we get bounded regions. The inclinations of the constraint regions can be understood from the relative sign between the parameters in the expressions for the EDMs. As expected the constraints for  $\Lambda = 1$  TeV are tighter than those for  $\Lambda = 5$  and 10 TeV and this is corroborated by the size of the coefficients entering in EDM expressions. In  $\Lambda = 1$  TeV case, the allowed values for parameters can reach  $\mathcal{O}(1)$  values at maximum. As we push the cutoff scale higher, the allowed range for parameters also increases. For example, for  $\Lambda = 10$  TeV the allowed values can become  $\mathcal{O}(10)$  or larger in some cases.

A naive comparison with the EDM calculation carried out in Ref. [49] with only  $\gamma\gamma h$  CP-odd coupling suggests that for  $\Lambda = 1$  TeV, the constraint equation for electron EDM measurement would be  $|\tilde{f}_{BB} + \tilde{f}_{WW}| \lesssim 0.0036$ . In the presence of CP-odd  $\gamma Zh$  coupling, which arises from same operators, this constraint equation would change. For example, our calculation for electron EDM constraint implies,  $|\tilde{f}_{BB} + 0.86\tilde{f}_{WW}| \lesssim 0.0026$ . In both the cases, the parameters would be allowed to take very large but fine-tuned values. However, we would like to point out that after including the constraints from the neutron EDM measurement, these parameters cannot take values larger than  $\mathcal{O}(0.1)$ .

When we take three parameters nonzero at a time, the parameters are scanned in the range -200 to 200. In Fig 9, we give two dimensional projection plots of the three dimensional constraint region for  $\Lambda = 1$  TeV. For comparison purpose, we present the plots in three categories discussed in the global analysis. We can see that with three parameters present, the constraints are more relaxed than when only two of them are nonzero. However, the parameters are still quite correlated.  $\tilde{f}_B$  and  $\tilde{f}_{BB}$  can often reach the boundary of the scanned regions. In fact it is very difficult to obtain closed boundaries. As we increase the range for parameter scan the allowed values for CP-odd parameters become very large [ $\mathcal{O}(1000)$ ]. However, it is important to note that for too large values of parameters, the two-loop EDM constraints may become relevant and, therefore, should also be taken into account. As we turn on more parameters, the correlation among parameters constrained by EDM is relaxed and the allowed parameter space also expands.

From the experimental perspective, a number of new EDM experiments promise to improve the level of sensitivity by one to two orders of magnitude in the coming years. For example, The Institut Laue Langevin (ILL) cryogenic experiment and the Spallation Neutron Source (SNS) nEDM experiment ([82], [83], [84]) aim at improving the upper limit on neutron EDM by two orders of magnitude, i.e down to  $\mathcal{O}(10^{-28})e.cm$ . This would imply that the numerical coefficients in the constraint equations for  $d_n$  in Eqs. (47), (48) and (49) would become stronger by almost two orders of magnitude and thus the allowed parameter space for  $\tilde{f}$ 's will be even more severely constrained, unless, of course, there is direct evidence of neutron EDM in the aforesaid experiments.

## 6 Discussion

We now highlight the important features of our analysis presented in sections 3, 4 and 5. We try to draw a comparative picture and address some of the issues relevant to the analysis.

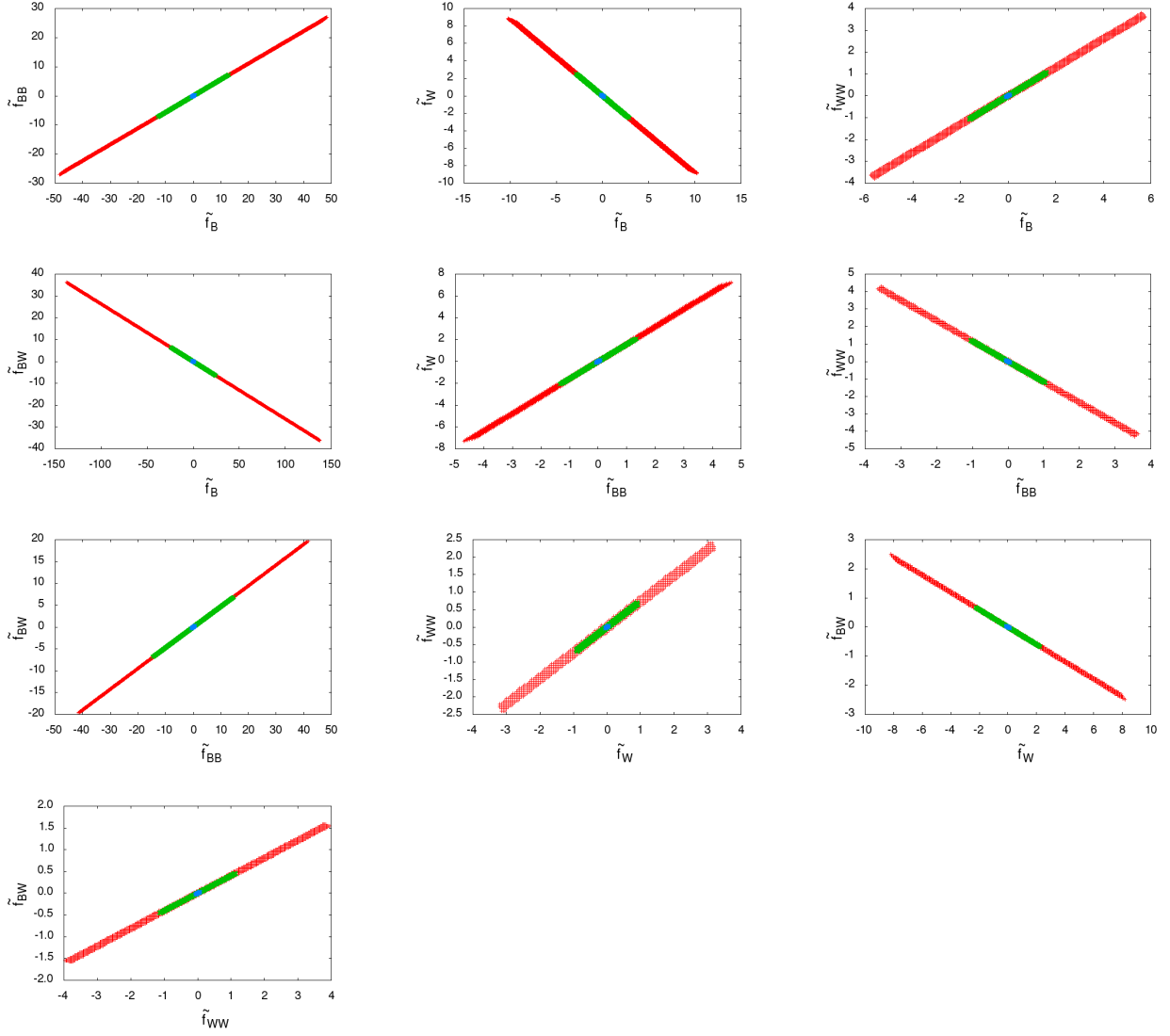


Figure 8: EDM constraints keeping two parameters nonzero at a time for three representative values of  $\Lambda = 1$ (blue), 5(green) & 10(red) TeV.

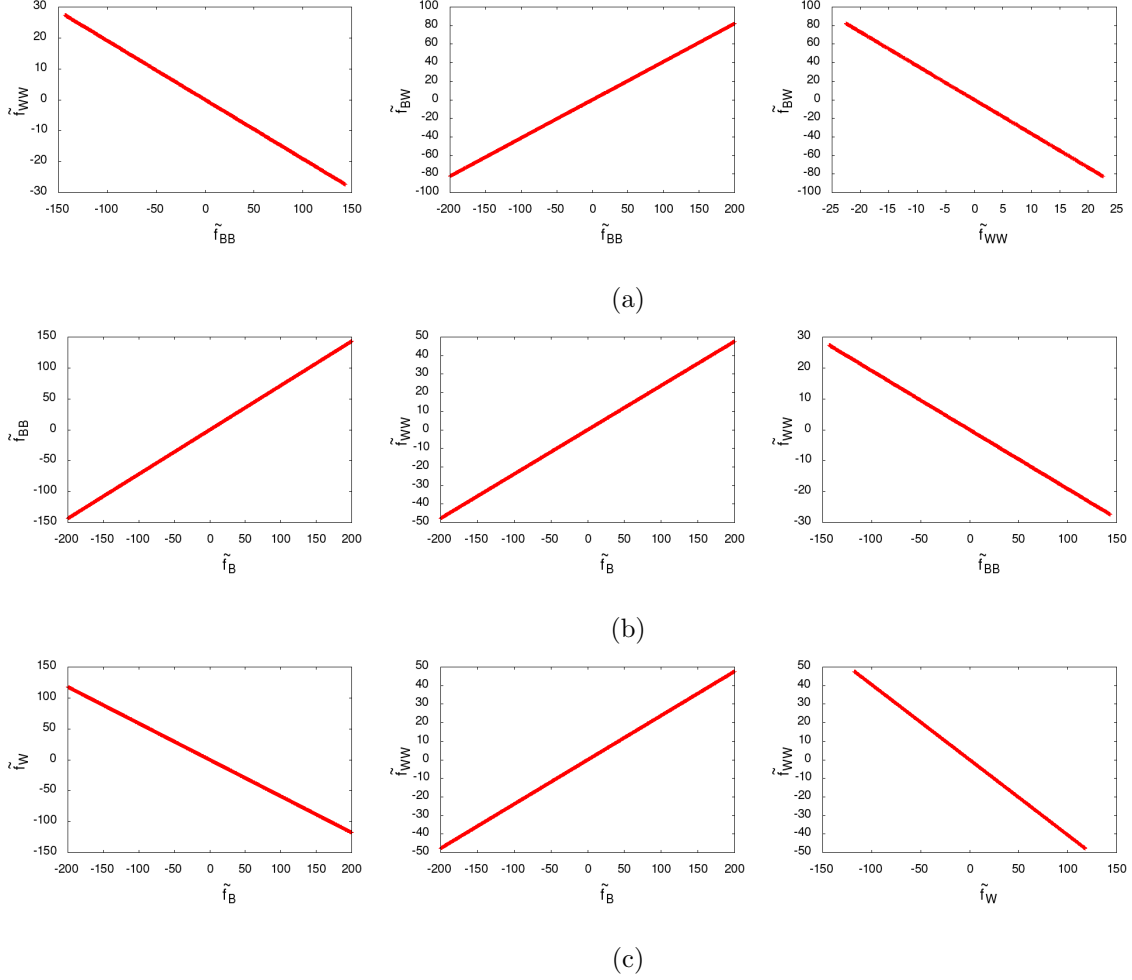


Figure 9: EDM constraints with (a)  $\tilde{f}_W = \tilde{f}_B = 0$ , (b)  $\tilde{f}_W = \tilde{f}_{BW} = 0$  and (c)  $\tilde{f}_{BB} = \tilde{f}_{BW} = 0$  for  $\Lambda = 1$  TeV. Parameters are varied in the range between -200 to 200.

- In the two parameter case, among all the constraints, the EWP constraints on CP-odd parameters are always the weakest while EDM constraints are the strongest. In general, the correlation among parameters is stronger in EWP and EDM cases as compared to the LHC case.
- In case of global fit of LHC data whatever contributes to  $h \rightarrow \gamma\gamma$  receives stronger constraints, since here the “tree level” contributions from the dimension six operators are essentially at the same level as the “one-loop” SM contributions. There are three such parameters namely  $\tilde{f}_{BB}$ ,  $\tilde{f}_{WW}$  and  $\tilde{f}_{BW}$ . Only a strong cancellation or correlation can keep the individual values of these parameters large.
- The same should apply to parameters contributing to  $h \rightarrow \gamma Z$  channel which also includes  $\tilde{f}_B$  and  $\tilde{f}_W$ . However the limits based on current data are rather weak there and we have not included them in our analysis. The global analysis puts some limits on  $\tilde{f}_B$  and  $\tilde{f}_W$  as the  $\gamma Zh$  coupling modifies the  $Zh$  and VBF production channels and the total Higgs decay width.
- The channels dependent on the  $WW h$  and  $ZZ h$  couplings yield relatively weak constraints from the global fits as a whole, since the higher dimensional interactions are inadequate to override the tree level SM contributions.
- In two parameter case, LHC data bounds on  $\tilde{f}_{BB}$ ,  $\tilde{f}_{BW}$  and  $\tilde{f}_{WW}$  are stronger when any of these is combined with  $\tilde{f}_B$  or  $\tilde{f}_W$ . These bounds are comparable to corresponding bounds obtained from EDM measurements.
- In three parameter case, the bounds from LHC data are stronger than those obtained from EDMs. In fact, for some parameters (for example,  $\tilde{f}_B$ ) values of the order 1000 are also allowed by EDM data. However, the parameters constrained from EDMs still display a tight correlation.
- If we allow dimension-6 CP-even operators to coexist with the CP-odd ones, the EWP and LHC observables would receive contributions at  $\mathcal{O}(1/\Lambda^2)$  (as a result of interference with the SM) as well as at  $\mathcal{O}(1/\Lambda^4)$ . Since there is no interference between CP-odd and CP-even operators in total rates, the CP-odd interactions studied by us should contribute to signal strengths on the order of  $(1/\Lambda^4)$ . For the sake of consistency, at  $\mathcal{O}(1/\Lambda^4)$  the contribution from dimension-8 CP-even operators via its interference with the SM should also be considered. Thus, in the presence of CP-even operators, the constraints from LHC and precision data can be relaxed. However, under the assumption that the effect of CP-conserving new physics is not significantly large, the constraints obtained by us on CP-odd operators are in a way the most conservative estimates of the allowed parameter space. Of course, the limits from EDM analyses remain the same in all the cases.
- A comparison between the relative strengths of the EDM and LHC constraints, we emphasize, is most transparent only when the CP-violating operators alone are considered, since the CP-conserving ones have no role in EDMs. Their inclusion, albeit via marginalization in the LHC global fits, will serve to relax the corresponding limits beyond what we have obtained. But then, it ceases to be a one-to-one comparison between the two kinds of constraints, something that we have intended to do from the beginning.

We have already seen that the Lorentz structure of anomalous CP-odd couplings is unique and these are just some linear combinations of the CP-odd parameters (see Table 1). Since in all

Couplings	LHC data		EDM	
	2P case	3P case	2P case	3P case
$ C_{WWh} $	0 – 60	0 – 60	0 – 0.17	0 – 55
$ C_{ZZh} $	25 – 100	25 – 80	0.11 – 0.20	0.15 – 33
$ C_{\gamma\gamma h} $	0 – 0.8	0 – 0.5	0 – 0.16	0.02 – 52
$ C_{\gamma Zh} $	20 – 25	15 – 25	0.03 – 0.25	0.05 – 110
$ C_{WW\gamma} $	0 – 40	15 – 40	0 – 0.15	0.02 – 47

Table 4: Limits on CP-odd coupling strengths from LHC data and EDM measurements for  $\Lambda=1$  TeV. 2P and 3P stand for two parameter nonzero and three parameter nonzero cases respectively.

the observables these couplings enter directly, it is instructive to know the kind of values these couplings can take as a result of our analysis presented above. In the calculation of  $S, T$  and  $U$  parameters all the CP-odd couplings directly enter. In the global analysis only  $C_{VVh}$  couplings participate, therefore, constraints on  $C_{WWV}$  from the LHC data are indirect. In EDM calculations only  $C_{\gamma\gamma h}, C_{\gamma Zh}$  and  $C_{WW\gamma}$  enter directly and therefore limits obtained on  $C_{WWh}$  and  $C_{ZZh}$  are also indirect. The limits on the strengths of the anomalous couplings are listed in Table 4. Since electroweak precision bounds on  $\tilde{f}_i$  are the weakest <sup>5</sup>, in the table we compare bounds on couplings due to LHC data and EDMs. The comparison is presented for both the two parameter (2P) and three parameter (3P) nonzero cases. Since  $C_{WWZ}$  is proportional to  $C_{WW\gamma}$ , the limits on  $C_{WW\gamma}$  can be easily translated to limits on  $C_{WWZ}$ . Looking at the LHC limits on the couplings we find that  $C_{\gamma\gamma h}$  is the most constrained coupling. Also, the LHC limits in 2P and 3P cases are comparable. On the other hand the EDM limits on couplings in 2P case is always stronger than in 3P case. In 3P case the lower limits result from the three parameter sets  $\{\tilde{f}_B, \tilde{f}_{BB}, \tilde{f}_{BW}\}$  and  $\{\tilde{f}_W, \tilde{f}_{WW}, \tilde{f}_{BW}\}$ . The parameters of these sets are found to be very fine tuned. It is important to recall that in 3P EDM case, the parameters are varied in the range between -200 to 200. We find that as we increase this range, the maximum allowed values for couplings also increase. We would also like to point out that the correlations among CP-odd couplings are mostly similar to those found among CP-odd parameters.

The triple gauge boson couplings (TGCs)  $WW\gamma$  and  $WWZ$  can also be constrained using the collider data on gauge boson pair production. Data from Tevatron and LHC are used mainly to constrain the CP-even anomalous couplings as the observables used are not sensitive to CP-odd couplings [85–90]. On the other hand, the experimental analyses at LEP which studied the angular distribution of final state particles are sensitive to CP-odd TGCs. A comparison between

<sup>5</sup>Although the EWP constraints are weaker in general, we find that the limits on  $C_{WWV}$  from EWP and LHC data are comparable in 2P case.

the CP-odd sector of TGC Lagrangian [54, 91, 92] and our effective Lagrangian (Eq. 2) implies

$$\frac{C_{WW\gamma}}{\Lambda^2} = \frac{s_W}{m_W^2} \tilde{\kappa}_\gamma \quad (50)$$

$$\frac{C_{WWZ}}{\Lambda^2} = \frac{c_W}{m_W^2} \tilde{\kappa}_Z. \quad (51)$$

Using the relation between  $C_{WW\gamma}$  and  $C_{WWZ}$  we get,  $\tilde{\kappa}_Z = -t_W^2 \tilde{\kappa}_\gamma$ . At 68% CL, the combined LEP limits on  $\tilde{\kappa}_Z$  are [79]

$$-0.14 \leq \tilde{\kappa}_Z \leq -0.06. \quad (52)$$

These limits when translated on  $C_{WWZ}$  and  $C_{WW\gamma}$  become,

$$\begin{aligned} -0.19 &\leq \frac{C_{WWZ}}{\Lambda^2} [\text{TeV}^{-2}] \leq -0.08, \\ 0.15 &\leq \frac{C_{WW\gamma}}{\Lambda^2} [\text{TeV}^{-2}] \leq 0.36. \end{aligned} \quad (53)$$

Note that these limits are comparable to the limits obtained from EDMs in 2P case, however, information on the sign of the couplings is also available.

Other than the  $VVh$  vertices considered in our analysis, quartic  $VVhh$  vertices also arise out of gauge invariant CP violating operators. One can thus expect some correlated phenomenology from the trilinear and quartic interactions, since the former arise essentially on replacing one Higgs by its vacuum expectation value in the quartic terms. In the analysis presented in this work, the production and decay channels considered are not affected at tree level by such quartic  $VVhh$  vertices. Thus in the context of the present analysis, any constraints on such quartic vertices from observed data are likely to be weaker than those obtained from the  $VVh(V = W, Z, \gamma)$  effective interactions, since the quartic couplings would entail Higgs pair production. For example, the  $VVhh$  vertex may contribute in addition to the  $hhh$  vertex toward a di-Higgs final state. However, one needs to wait for a large volume of data on Higgs pair production to see such correlated phenomena. In general, limits stronger than what we have obtained are not expected. Also, the contributions from such  $VVhh$  CP-odd vertices to EDMs and EWP observables come at higher loop levels and thus are expected to be substantially weaker than what we have obtained for the trilinear terms.

It is a well-known fact that the observed baryon asymmetry in our universe cannot be explained by just the CP-violating phase of the Cabibbo-Kobayashi-Maskawa (CKM) matrix in the SM. The presence of additional sources of CP-violating operators arising from the anomalous  $VVh$  interactions may in principle explain the observed baryon asymmetry of the universe. However, a more careful scrutiny of this picture reveals that our CP-violating operators are not sufficient to trigger strongly the first order electroweak phase transition required for the baryogenesis. For this, one has to extend the Higgs sector of the SM by introducing new particles which couple to the Higgs boson and thus modify the Higgs potential such that it leads to a strongly first order electroweak phase transition [93].

## 7 Summary and Conclusions

We have analyzed CP-odd  $VVh(V = W, Z, \gamma)$  and  $WWV(V = Z, \gamma)$  interactions in terms of gauge invariant dimension-6 operators, obtained as the artifacts of physics beyond the standard model. The most complete set, comprising five gauge-Higgs operators, has been taken into account. We have derived constraints on the coefficients of such operators using electroweak precision data,



LHC data on Higgs and limits on the electric dipole moments of the neutron and the electron. With  $\Lambda$  as the scale suppressing the CP-violating operators, precision parameters as well as LHC observables receive contributions  $\sim 1/\Lambda^4$  from the CP-odd couplings, while contributions  $\sim 1/\Lambda^2$  to EDM observables are expected. The constraints obtained from the  $S, T$  and  $U$  parameters are the weakest, while the bounds from EDMs are the strongest with two nonvanishing operators. The global analysis of Higgs data from the LHC puts stronger constraints on those CP-odd effective couplings which contribute to  $h \rightarrow \gamma\gamma$ , as compared to those which do not. We also indicate situations where large values of certain couplings are allowed by all constraints, when they appear in combination. The constraints coming from LEP on CP-odd form factors  $C_{WW\gamma}$  and  $C_{WWZ}$  are consistent with our limits obtained from EDMs in the case when any two out of five parameters are nonzero. It may be of interest to find out new physics scenarios where, by integrating out heavy degrees of freedom, one may arrive at large correlated values of such operators. In a subsequent work, [94] we hope to discuss some observables that may help one in probing these operators in the 13 and 14 TeV LHC runs.

## Acknowledgements

We thank Shankha Banerjee, Jyotiranjana Beuria, Nabarun Chakraborty, Arghya Choudhury, Anushree Ghosh and Tanumoy Mandal for fruitful discussions. The work of S.D., B.M. and A.S. is partially supported by funding available from the Department of Atomic Energy, Government of India, for the Regional Centre for Accelerator-based Particle Physics (RECAPP), Harish-Chandra Research Institute. D.K.G. would like to acknowledge the hospitality of RECAPP at the initial stage of this project. B.M. acknowledges the hospitality of Indian Association for the Cultivation of Science, Kolkata. A.S. would like to thank CP3-Louvain, Belgium for hospitality while part of the work was carried out.

## Appendix A Gauge boson two-point functions in presence of CP-odd couplings

We define the two-point function for electroweak gauge bosons  $V_1$  and  $V_2$  as,

$$\Pi_{V_1 V_2}^{\mu\nu}(p^2) = g^{\mu\nu} \Pi_{V_1 V_2}(p^2) + p^\mu p^\nu \tilde{\Pi}_{V_1 V_2}(p^2). \quad (54)$$

In electroweak precision observables only  $\Pi_{V_1 V_2}(p^2)$  contribute. Below we give their expressions due to CP-odd couplings in terms of one-loop scalar functions  $A_0$  and  $B_0$ .

$$\begin{aligned} \Pi_{\gamma\gamma}(p^2) = & \frac{g^2 m_W^2}{18\Lambda^4} \left( 3p^2 (C_{\gamma\gamma h}^2 (2m_h^2 - p^2) B_0(p^2, 0, m_h^2) - 2C_{WW\gamma}^2 (2m_W^2 + p^2) B_0(p^2, m_W^2, m_W^2)) \right. \\ & + C_{\gamma Zh}^2 A_0(m_Z^2) + 4C_{WW\gamma}^2 A_0(m_W^2) - 3C_{\gamma\gamma h}^2 m_h^4 B_0(p^2, 0, m_h^2) - 3C_{\gamma Zh}^2 (m_h^4 - 2m_h^2 (m_Z^2 + p^2) \\ & + (m_Z^2 - p^2)^2) B_0(p^2, m_Z^2, m_h^2) + 3A_0(m_h^2) (C_{\gamma\gamma h}^2 (m_h^2 + p^2) + C_{\gamma Zh}^2 (m_h^2 - m_Z^2 + p^2)) \\ & + 3C_{\gamma Zh}^2 A_0(m_Z^2) (m_Z^2 - m_h^2) + p^2 (7C_{\gamma\gamma h}^2 (p^2 - 3m_h^2) + 7C_{\gamma Zh}^2 (p^2 - 3(m_h^2 + m_Z^2))) \\ & \left. + 2C_{WW\gamma}^2 (12m_W^2 + 7p^2) \right), \end{aligned} \quad (55)$$

$$\begin{aligned}
\Pi_{\gamma Z}(p^2) = & \frac{g^2 m_W^2}{18\Lambda^4} \left( -3C_{\gamma\gamma h} C_{\gamma Zh} (m_h^2 - p^2)^2 B_0(p^2, 0, m_h^2) - 3C_{\gamma Zh} C_{ZZh} (m_h^4 - 2m_h^2 (m_Z^2 + p^2) \right. \\
& + (m_Z^2 - p^2)^2) B_0(p^2, m_Z^2, m_h^2) - 6C_{WW\gamma} C_{WWZ} p^2 (2m_W^2 + p^2) B_0(p^2, m_W^2, m_W^2) \\
& + 3C_{\gamma Zh} A_0(m_h^2) (C_{\gamma\gamma h} (m_h^2 + p^2) + C_{ZZh} (m_h^2 - m_Z^2 + p^2)) + 3C_{\gamma Zh} C_{ZZh} A_0(m_Z^2) \\
& (-m_h^2 + m_Z^2 + p^2) + 12C_{WW\gamma} C_{WWZ} p^2 A_0(m_W^2) + p^2 (7p^2 (C_{\gamma Zh} (C_{\gamma\gamma h} + C_{ZZh}) \\
& + 2C_{WW\gamma} C_{WWZ}) - 21C_{\gamma Zh} (m_h^2 (C_{\gamma\gamma h} + C_{ZZh}) + C_{ZZh} m_Z^2) + 24C_{WW\gamma} C_{WWZ} m_W^2) \Big), \tag{56}
\end{aligned}$$

$$\begin{aligned}
\Pi_{ZZ}(p^2) = & \frac{g^2 m_W^2}{18\Lambda^4} \left( 3p^2 (C_{\gamma Zh}^2 (2m_h^2 - p^2) B_0(p^2, 0, m_h^2) - 2C_{WWZ}^2 (2m_W^2 + p^2) B_0(p^2, m_W^2, m_W^2) \right. \\
& + 4C_{WWZ}^2 A_0(m_W^2) + C_{ZZh}^2 A_0(m_Z^2)) - 3C_{\gamma Zh}^2 m_h^4 B_0(p^2, 0, m_h^2) - 3C_{ZZh}^2 (m_h^4 - 2m_h^2 (m_Z^2 + p^2) \\
& + (m_Z^2 - p^2)^2) B_0(p^2, m_Z^2, m_h^2) + 3A_0(m_h^2) (C_{\gamma Zh}^2 (m_h^2 + p^2) + C_{ZZh}^2 (m_h^2 - m_Z^2 + p^2)) \\
& + 3C_{ZZh}^2 A_0(m_Z^2) (m_Z^2 - m_h^2) + p^2 (7C_{\gamma Zh}^2 (p^2 - 3m_h^2) + 2C_{WWZ}^2 (12m_W^2 + 7p^2) \\
& + 7C_{ZZh}^2 (p^2 - 3(m_h^2 + m_Z^2))) \Big), \tag{57}
\end{aligned}$$

$$\begin{aligned}
\Pi_{WW}(p^2) = & \frac{g^2 m_W^2}{18\Lambda^4 p^2} \left( 3 \left( -C_{WW\gamma}^2 (m_W^2 - p^2)^2 (m_W^2 + p^2) B_0(p^2, m_W^2, 0) + C_{WW h}^2 (-p^2) (m_h^4 \right. \right. \\
& - 2m_h^2 (m_W^2 + p^2) + (m_W^2 - p^2)^2) B_0(p^2, m_W^2, m_h^2) - C_{WWZ}^2 (m_W^6 - m_W^4 (2m_Z^2 + p^2) \\
& + m_W^2 (m_Z^4 + 8m_Z^2 p^2 - (p^2)^2) + p^2 (m_Z^2 - p^2)^2) B_0(p^2, m_W^2, m_Z^2) - C_{WWZ}^2 A_0(m_Z^2) (m_W^2 + p^2) \\
& (m_W^2 - m_Z^2 - p^2)) + 3A_0(m_W^2) (C_{WW\gamma}^2 (m_W^4 - 10m_W^2 p^2 + (p^2)^2) + C_{WW h}^2 p^2 (-m_h^2 + m_W^2 + p^2) \\
& + C_{WWZ}^2 (m_W^4 - m_W^2 (m_Z^2 + 10p^2) + p^2 (p^2 - m_Z^2))) + 3C_{WW h}^2 p^2 A_0(m_h^2) (m_h^2 - m_W^2 + p^2) \\
& + p^2 (C_{WW\gamma}^2 (87m_W^4 - 14m_W^2 p^2 + 7(p^2)^2) + 7C_{WW h}^2 p^2 (p^2 - 3(m_h^2 + m_W^2)) + C_{WWZ}^2 \\
& (-7p^2 (2m_W^2 + 3m_Z^2) + 87m_W^2 (m_W^2 + m_Z^2) + 7(p^2)^2)) \Big). \tag{58}
\end{aligned}$$

Out of these,  $\Pi_{\gamma\gamma}$ ,  $\Pi_{\gamma Z}$  and  $\Pi_{ZZ}$  vanish at  $p^2 = 0$ . Note that in  $\Pi_{WW}$  there is an overall  $1/p^2$  dependence. We would like to mention that both  $\Pi_{WW}$  and its derivative converge smoothly in  $p^2 \rightarrow 0$  limit. The one-loop scalar functions in  $n = 4 - 2\epsilon$  dimensions are given by,

$$\begin{aligned}
A_0(m_0^2) &= \int \frac{d^n l}{(2\pi)^n} \frac{1}{l^2 - m_0^2} \\
&\equiv \frac{1}{16\pi^2} m_0^2 \left[ \frac{1}{\epsilon} + 1 - \ln(m_0^2) \right], \tag{59}
\end{aligned}$$

$$\begin{aligned}
B_0(p^2, m_0^2, m_1^2) &= \int \frac{d^n l}{(2\pi)^n} \frac{1}{(l^2 - m_0^2) ((l+p)^2 - m_1^2)} \\
&\equiv \frac{1}{16\pi^2} \left[ \frac{1}{\epsilon} - \Delta(p^2, m_0^2, m_1^2) \right], \tag{60}
\end{aligned}$$

where,

$$\Delta(p^2, m_0^2, m_1^2) = \int_0^1 dx \ln [-x(1-x)p^2 + x(m_1^2 - m_0^2) + m_0^2]. \tag{61}$$

This form is suitable for computing  $B_0$  and its derivative with respect to  $p^2$  at  $p^2 = 0$ , which we require to calculate  $S, T$  and  $U$  parameters discussed in section 3.

## References

- [1] G. Aad *et al.* [ATLAS Collaboration], Phys. Lett. B **716**, 1 (2012) [arXiv:1207.7214 [hep-ex]].
- [2] S. Chatrchyan *et al.* [CMS Collaboration], Phys. Lett. B **716**, 30 (2012) [arXiv:1207.7235 [hep-ex]].
- [3] P. P. Giardino, K. Kannike, M. Raidal and A. Strumia, JHEP **1206**, 117 (2012) [arXiv:1203.4254 [hep-ph]].
- [4] M. Klute, R. Lafaye, T. Plehn, M. Rauch and D. Zerwas, Phys. Rev. Lett. **109**, 101801 (2012) [arXiv:1205.2699 [hep-ph]].
- [5] S. Banerjee, S. Mukhopadhyay and B. Mukhopadhyaya, JHEP **1210**, 062 (2012) [arXiv:1207.3588 [hep-ph]].
- [6] M. B. Einhorn and J. Wudka, Nucl. Phys. B **877**, 792 (2013) [arXiv:1308.2255 [hep-ph]].
- [7] M. Baak *et al.* [Gfitter Group Collaboration], Eur. Phys. J. C **74**, 3046 (2014) [arXiv:1407.3792 [hep-ph]].
- [8] W. Buchmuller and D. Wyler, Nucl. Phys. B **268**, 621 (1986).
- [9] B. Grzadkowski, M. Iskrzynski, M. Misiak and J. Rosiek, JHEP **1010**, 085 (2010) [arXiv:1008.4884 [hep-ph]].
- [10] J. R. Espinosa, C. Grojean, M. Muhlleitner and M. Trott, JHEP **1205**, 097 (2012) [arXiv:1202.3697 [hep-ph]].
- [11] A. Azatov, R. Contino and J. Galloway, JHEP **1204**, 127 (2012) [JHEP **1304**, 140 (2013)] [arXiv:1202.3415 [hep-ph]].
- [12] R. Contino, M. Ghezzi, C. Grojean, M. Muhlleitner and M. Spira, JHEP **1307**, 035 (2013) [arXiv:1303.3876 [hep-ph]].
- [13] F. Maltoni, K. Mawatari and M. Zaro, Eur. Phys. J. C **74**, no. 1, 2710 (2014) [arXiv:1311.1829 [hep-ph]].
- [14] E. Masso, JHEP **1410**, 128 (2014) [arXiv:1406.6376 [hep-ph]].
- [15] A. Falkowski, arXiv:1505.00046 [hep-ph].
- [16] M. C. Gonzalez-Garcia, Int. J. Mod. Phys. A **14**, 3121 (1999) [hep-ph/9902321].
- [17] T. Han and J. Jiang, Phys. Rev. D **63**, 096007 (2001) [hep-ph/0011271].
- [18] T. Plehn, D. L. Rainwater and D. Zeppenfeld, Phys. Rev. Lett. **88**, 051801 (2002) [hep-ph/0105325].
- [19] V. Barger, T. Han, P. Langacker, B. McElrath and P. Zerwas, Phys. Rev. D **67**, 115001 (2003) [hep-ph/0301097].

- [20] S. S. Biswal, R. M. Godbole, R. K. Singh and D. Choudhury, Phys. Rev. D **73**, 035001 (2006) [Phys. Rev. D **74**, 039904 (2006)] [hep-ph/0509070].
- [21] T. Han, Y. P. Kuang and B. Zhang, Phys. Rev. D **73**, 055010 (2006) [hep-ph/0512193].
- [22] R. M. Godbole, S. Kraml, S. D. Rindani and R. K. Singh, Phys. Rev. D **74**, 095006 (2006) [Phys. Rev. D **74**, 119901 (2006)] [hep-ph/0609113].
- [23] R. M. Godbole, D. J. Miller and M. M. Muhlleitner, JHEP **0712**, 031 (2007) [arXiv:0708.0458 [hep-ph]].
- [24] S. S. Biswal and R. M. Godbole, Phys. Lett. B **680**, 81 (2009) [arXiv:0906.5471 [hep-ph]].
- [25] N. D. Christensen, T. Han and Y. Li, Phys. Lett. B **693**, 28 (2010) [arXiv:1005.5393 [hep-ph]].
- [26] N. Desai, D. K. Ghosh and B. Mukhopadhyaya, Phys. Rev. D **83**, 113004 (2011) [arXiv:1104.3327 [hep-ph]].
- [27] A. Freitas and P. Schwaller, Phys. Rev. D **87**, no. 5, 055014 (2013) [arXiv:1211.1980 [hep-ph]].
- [28] W. Dekens and J. de Vries, JHEP **1305**, 149 (2013) [arXiv:1303.3156 [hep-ph]].
- [29] C. Y. Chen, S. Dawson and C. Zhang, Phys. Rev. D **89**, no. 1, 015016 (2014) [arXiv:1311.3107 [hep-ph]].
- [30] S. S. Biswal, R. M. Godbole, B. Mellado and S. Raychaudhuri, Phys. Rev. Lett. **109**, 261801 (2012) [arXiv:1203.6285 [hep-ph]].
- [31] I. Low, J. Lykken and G. Shaughnessy, Phys. Rev. D **86**, 093012 (2012) [arXiv:1207.1093 [hep-ph]].
- [32] E. Mass and V. Sanz, Phys. Rev. D **87**, no. 3, 033001 (2013) [arXiv:1211.1320 [hep-ph]].
- [33] A. Djouadi and G. Moreau, Eur. Phys. J. C **73**, no. 9, 2512 (2013) [arXiv:1303.6591 [hep-ph]].
- [34] I. T. Cakir, O. Cakir, A. Senol and A. T. Tasci, Mod. Phys. Lett. A **28**, no. 31, 1350142 (2013) [arXiv:1304.3616 [hep-ph]].
- [35] R. Godbole, D. J. Miller, K. Mohan and C. D. White, Phys. Lett. B **730**, 275 (2014) [arXiv:1306.2573 [hep-ph]].
- [36] S. Banerjee, S. Mukhopadhyay and B. Mukhopadhyaya, Phys. Rev. D **89**, no. 5, 053010 (2014) [arXiv:1308.4860 [hep-ph]].
- [37] I. Anderson, S. Bolognesi, F. Caola, Y. Gao, A. V. Gritsan, C. B. Martin, K. Melnikov and M. Schulze *et al.*, Phys. Rev. D **89**, no. 3, 035007 (2014) [arXiv:1309.4819 [hep-ph]].
- [38] R. M. Godbole, D. J. Miller, K. A. Mohan and C. D. White, JHEP **1504**, 103 (2015) [arXiv:1409.5449 [hep-ph]].
- [39] V. Khachatryan *et al.* [CMS Collaboration], arXiv:1411.3441 [hep-ex].
- [40] J. Ellis, V. Sanz and T. You, JHEP **1407**, 036 (2014) [arXiv:1404.3667 [hep-ph]].
- [41] Y. Chen, A. Falkowski, I. Low and R. Vega-Morales, Phys. Rev. D **90**, no. 11, 113006 (2014) [arXiv:1405.6723 [hep-ph]].

- [42] A. V. Manohar and M. B. Wise, Phys. Lett. B **636**, 107 (2006) [hep-ph/0601212].
- [43] T. Corbett, O. J. P. Eboli, J. Gonzalez-Fraile and M. C. Gonzalez-Garcia, Phys. Rev. D **86**, 075013 (2012) [arXiv:1207.1344 [hep-ph]].
- [44] T. Corbett, O. J. P. Eboli, J. Gonzalez-Fraile and M. C. Gonzalez-Garcia, Phys. Rev. D **87**, 015022 (2013) [arXiv:1211.4580 [hep-ph]].
- [45] W. -F. Chang, W. -P. Pan and F. Xu, Phys. Rev. D **88**, no. 3, 033004 (2013) [arXiv:1303.7035 [hep-ph]].
- [46] B. Gripaios and D. Sutherland, Phys. Rev. D **89**, no. 7, 076004 (2014) [arXiv:1309.7822 [hep-ph]].
- [47] H. Belusca-Maito, arXiv:1404.5343 [hep-ph].
- [48] A. Falkowski and F. Riva, JHEP **1502**, 039 (2015) [arXiv:1411.0669 [hep-ph]].
- [49] D. McKeen, M. Pospelov and A. Ritz, Phys. Rev. D **86**, 113004 (2012) [arXiv:1208.4597 [hep-ph]].
- [50] K. A. Olive *et al.* [Particle Data Group Collaboration], Chin. Phys. C **38**, 090001 (2014).
- [51] A. D. Sakharov, Pisma Zh. Eksp. Teor. Fiz. **5**, 32 (1967) [JETP Lett. **5**, 24 (1967)] [Sov. Phys. Usp. **34**, 392 (1991)] [Usp. Fiz. Nauk **161**, 61 (1991)].
- [52] A. Riotto, hep-ph/9807454.
- [53] M. B. Voloshin, Phys. Rev. D **86**, 093016 (2012) [arXiv:1208.4303 [hep-ph]].
- [54] M. B. Gavela, J. Gonzalez-Fraile, M. C. Gonzalez-Garcia, L. Merlo, S. Rigolin and J. Yepes, JHEP **1410**, 44 (2014) [arXiv:1406.6367 [hep-ph]].
- [55] J. Yepes, R. Kunming and J. Shu, arXiv:1507.04745 [hep-ph].
- [56] C. S. Lim, Phys. Lett. B **256**, 233 (1991).
- [57] C. S. Lim, N. Maru and K. Nishiwaki, Phys. Rev. D **81**, 076006 (2010) [arXiv:0910.2314 [hep-ph]].
- [58] R. D. Peccei and H. R. Quinn, Phys. Rev. Lett. **38**, 1440 (1977).
- [59] R. D. Peccei and H. R. Quinn, Phys. Rev. D **16**, 1791 (1977).
- [60] M. E. Peskin and T. Takeuchi, Phys. Rev. D **46**, 381 (1992).
- [61] J. Alwall, R. Frederix, S. Frixione, V. Hirschi, F. Maltoni, O. Mattelaer, H.-S. Shao and T. Stelzer *et al.*, JHEP **1407**, 079 (2014) [arXiv:1405.0301 [hep-ph]].
- [62] N. D. Christensen and C. Duhr, Comput. Phys. Commun. **180**, 1614 (2009) [arXiv:0806.4194 [hep-ph]].
- [63] J. Pumplin, D. R. Stump, J. Huston, H. L. Lai, P. M. Nadolsky and W. K. Tung, JHEP **0207**, 012 (2002) [hep-ph/0201195].
- [64] <https://twiki.cern.ch/twiki/bin/view/LHCPhysics/CrossSections>

- [65] S. Chatrchyan *et al.* [CMS Collaboration], Phys. Lett. B **726**, 587 (2013) [arXiv:1307.5515 [hep-ex]].
- [66] G. Aad *et al.* [ATLAS Collaboration], Phys. Lett. B **732**, 8 (2014) [arXiv:1402.3051 [hep-ex]].
- [67] G. Aad *et al.* [ATLAS Collaboration], arXiv:1408.7084 [hep-ex].
- [68] V. Khachatryan *et al.* [CMS Collaboration], arXiv:1407.0558 [hep-ex].
- [69] G. Aad *et al.* [ATLAS Collaboration], Phys. Rev. D **91**, no. 1, 012006 (2015) [arXiv:1408.5191 [hep-ex]].
- [70] S. Chatrchyan *et al.* [CMS Collaboration], Phys. Rev. D **89**, no. 9, 092007 (2014) [arXiv:1312.5353 [hep-ex]].
- [71] ATLAS-CONF-2014-060.
- [72] S. Chatrchyan *et al.* [CMS Collaboration], JHEP **1401**, 096 (2014) [arXiv:1312.1129 [hep-ex]].
- [73] V. Khachatryan *et al.* [CMS Collaboration], Phys. Lett. B **736**, 64 (2014) [arXiv:1405.3455 [hep-ex]].
- [74] C. Englert, A. Freitas, M. M. Mhlleitner, T. Plehn, M. Rauch, M. Spira and K. Walz, J. Phys. G **41**, 113001 (2014) [arXiv:1403.7191 [hep-ph]].
- [75] M. Pospelov and A. Ritz, Annals Phys. **318**, 119 (2005) [hep-ph/0504231].
- [76] J. Engel, M. J. Ramsey-Musolf and U. van Kolck, Prog. Part. Nucl. Phys. **71**, 21 (2013) [arXiv:1303.2371 [nucl-th]].
- [77] A. Czarnecki and B. Krause, Phys. Rev. Lett. **78**, 4339 (1997) [hep-ph/9704355].
- [78] J. Baron *et al.* [ACME Collaboration], Science **343**, no. 6168, 269 (2014) [arXiv:1310.7534 [physics.atom-ph]].
- [79] J. Beringer *et al.* [Particle Data Group Collaboration], Phys. Rev. D **86**, 010001 (2012).
- [80] C. A. Baker, D. D. Doyle, P. Geltenbort, K. Green, M. G. D. van der Grinten, P. G. Harris, P. Iaydjiev and S. N. Ivanov *et al.*, Phys. Rev. Lett. **97**, 131801 (2006) [hep-ex/0602020].
- [81] C. Dib, A. Faessler, T. Gutsche, S. Kovalenko, J. Kuckei, V. E. Lyubovitskij and K. Pumsaard, J. Phys. G **32**, 547 (2006) [hep-ph/0601144].
- [82] J. C. Peng, Mod. Phys. Lett. A **23**, 1397 (2008) [arXiv:0804.4254 [nucl-ex]].
- [83] T. M. Ito, J. Phys. Conf. Ser. **69**, 012037 (2007) [nucl-ex/0702024 [NUCL-EX]].
- [84] M. Raidal *et al.*, Eur. Phys. J. C **57**, 13 (2008) [arXiv:0801.1826 [hep-ph]].
- [85] H. T. Diehl [CDF and D0 Collaborations], In \*Vancouver 1998, High energy physics, vol. 1\* 520-524 [hep-ex/9810006].
- [86] V. M. Abazov *et al.* [D0 Collaboration], Phys. Rev. Lett. **107**, 241803 (2011) [arXiv:1109.4432 [hep-ex]].

- [87] G. Aad *et al.* [ATLAS Collaboration], Eur. Phys. J. C **72**, 2173 (2012) [arXiv:1208.1390 [hep-ex]].
- [88] G. Aad *et al.* [ATLAS Collaboration], Phys. Rev. D **87** (2013) 11, 112001 [Erratum-ibid. D **88** (2013) 7, 079906] [arXiv:1210.2979 [hep-ex]].
- [89] S. Chatrchyan *et al.* [CMS Collaboration], Eur. Phys. J. C **73**, 2610 (2013) [arXiv:1306.1126 [hep-ex]].
- [90] S. Chatrchyan *et al.* [CMS Collaboration], Phys. Rev. D **89**, no. 9, 092005 (2014) [arXiv:1308.6832 [hep-ex]].
- [91] K. Hagiwara, R. D. Peccei, D. Zeppenfeld and K. Hikasa, Nucl. Phys. B **282**, 253 (1987).
- [92] S. Dawson, S. K. Gupta and G. Valencia, Phys. Rev. D **88**, no. 3, 035008 (2013) [arXiv:1304.3514 [hep-ph]].
- [93] D. E. Morrissey, and M. J. Ramsey-Musolf, New J. Phys., **14**,125003,(2012); arXiv:1206.2942 and references therein.
- [94] S. Dwivedi, D. K. Ghosh, B. Mukhopadhyaya and A. Shivaji, *In preparation*.